LAWRENCE
LIVERMORE
NATIONAL
LABORATORY

LLNL-TR-691810

California GAMA Special Study: Tracers of recent recharge to predict drought impacts on groundwater: Mount Shasta Study Area

Ate Visser, Jean E. Moran*, Amanda Deinhart, Elizabeth Peters, Richard Bibby, and Bradley K. Esser

Lawrence Livermore National Laboratory
**California State University, East Bay*

December 2016

Draft Report for the California State Water Resources Control Board

GAMA Special Studies Task 15.2: *Tracers of recent recharge to predict drought impacts on groundwater*

Disclaimer

Auspices Statement

This work performed under the auspices of the U.S. Department of Energy by Lawrence Livermore National Laboratory under Contract DE-AC52-07NA27344.

GAMA: GROUNDWATER AMBIENT MONITORING & ASSESSMENT PROGRAM SPECIAL STUDY

California GAMA Special Study:
Tracers of recent recharge to predict drought impacts on groundwater: Mount Shasta Study Area

Ate Visser, Jean E. Moran, Amanda Deinhart,*
Elizabeth Peters, Richard Bibby, and Bradley K. Esser*

Lawrence Livermore National Laboratory
**California State University, East Bay*

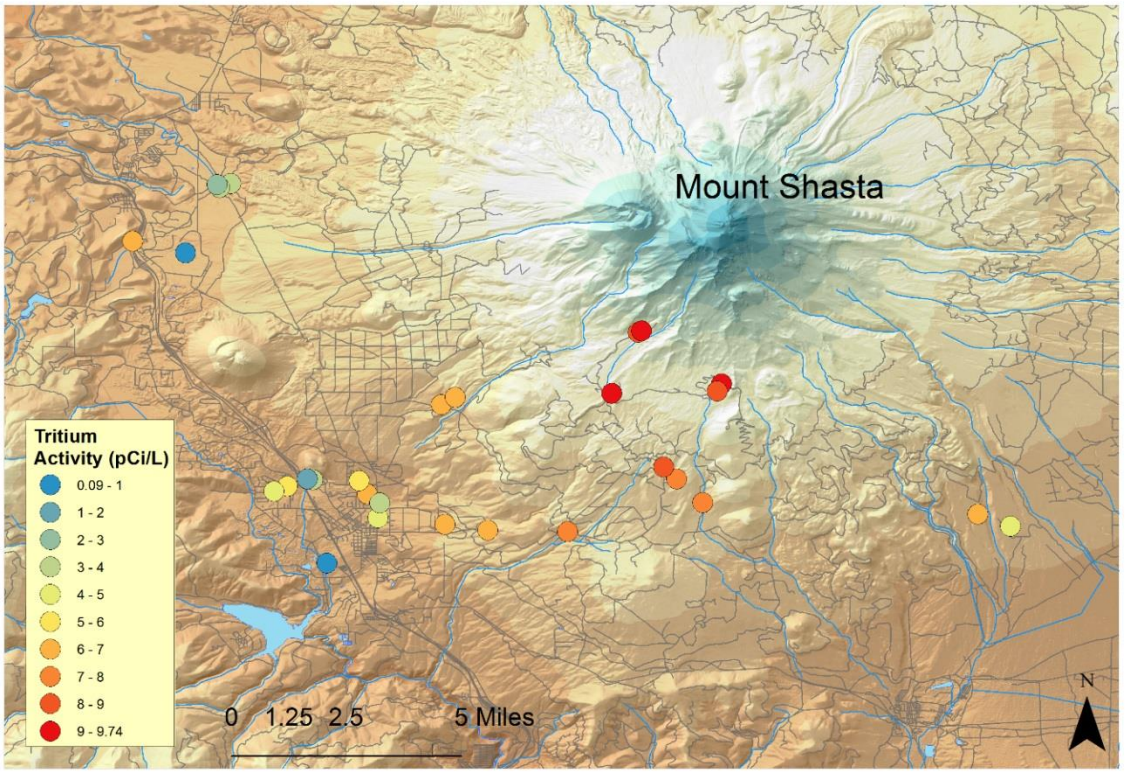

Prepared in cooperation with the
California State Water Resource Control Board
LLNL-TR-691810

December 2016

Suggested citation:
Ate Visser, Jean E. Moran, Amanda Deinhart, Elizabeth Peters, Richard Bibby, and Bradley K. Esser (2016) **California GAMA Special Study: Tracers of recent recharge to predict drought impacts on groundwater: Mount Shasta Study Area**. Lawrence Livermore National Laboratory LLNL-TR-691810, 43 pp.

California GAMA Special Study: Tracers of recent recharge to predict drought impacts on groundwater: Mount Shasta Study Area

A. Visser, J. E. Moran*, Amanda Deinhart, Elizabeth Peters*, Richard Bibby, and B. K. Esser:
*Lawrence Livermore National Laboratory, *California State University-East Bay*
Prepared in cooperation with the State Water Resources Control Board

Key Points

- Wells and springs on and around Mount Shasta were sampled and analyzed for a suite of geochemical and isotopic tracers to examine recharge areas, water flow paths, and subsurface residence times. Samples were collected during a time of extreme drought (May-September, 2015), following three years of below-average snowfall.
- Noble gas composition and $\delta^{18}O$ signatures indicate that sampled springs and wells produce water that recharged between 2000 m and 3000 m elevation.
- A fraction of the water in lower elevation springs and wells (discharging below 1500 m elevation) recharged through forested soils with biological activity, based on the carbon isotopic signature. Exclusive recharge above the tree line (2500 m) is therefore not a likely scenario for sampled groundwater. However, high elevation wells and springs show a carbon isotopic signature closer to atmospheric, indicative of recharge through bare land surface.
- Groundwater flow path depths of 500 m are calculated from temperature differences between recharge and discharge, which are the result of geothermal and gravitational heating.
- Anion chemistry of sampled water shows three distinct groupings, dominated by chloride, sulfate or bicarbonate, in the west, north and south side of the study area respectively.
- Carbon and helium isotopic signatures indicate contributions of mantle-derived fluids in wells. Radiogenic (crustal) helium is also found in a few samples.
- Newly developed groundwater age isotopic tracers ^{35}S and ^{22}Na with short half-lives (87.4 d and 2.6 yr, respectively) indicate that the groundwater sampled for these isotopes has a residence time longer than the dating range of these tracers (2 yr and 5 yr, respectively).
- Apparent groundwater ages, based on ^{3}H, ^{85}Kr and/or $^{3}H/^{3}He$ are determined for a few wells, and are one to four decades. One well and one spring produce water with an age greater than 50 years.
- A spatial analysis of precipitation, evapotranspiration and land cover confirms the conclusions based on isotopic results, i.e., water from elevations above 2000 m contributes disproportionately to groundwater recharge due to higher precipitation rates and lower evapotranspiration rates.
- The spatial analysis also indicates that lower elevations (below 2000 m) contribute more than 50% of total recharge in the study area, despite lower precipitation and higher evapotranspiration rates, due to a larger land surface area in this elevation range.

California GAMA Special Study: Tracers of recent recharge to predict drought impacts on groundwater: Mount Shasta Study Area

A. Visser, J. E. Moran*, Amanda Deinhart, Elizabeth Peters*, Richard Bibby, and B. K. Esser:
*Lawrence Livermore National Laboratory, *California State University-East Bay*
Prepared in cooperation with the State Water Resources Control Board

Table of Contents

1 INTRODUCTION

Mount Shasta (4322 m) is the most voluminous (350 km^3) stratovolcano in the Cascade Volcanic Arc and is famous for its spring water (Figure 1). On Mount Shasta, most precipitation falls as snow above 1500 m. Municipal, domestic and industrial water supply is obtained from local springs and wells, which discharge from an aquifer system comprising deposits of young volcanic formations. There is limited information about the storage capacity of the aquifer system, due to the unpredictable nature of the geometry and lithology of volcanic deposits. In the city of Mount Shasta, residential water use was estimated at 120 gallons per person per day in May 2015, achieving water savings of 50% compared to May 2013 (California SWRCB, 2016). Additional water is used in the logging industry, and exported from the area in the form of bottled water. Since runoff from Mount Shasta forms the headwaters of the Upper Sacramento River, water usage in Mount Shasta, under conditions of drought and climate change, may impact cities near Mount Shasta, as well as areas south of Mount Shasta that depend on Sacramento River water.

The Groundwater Ambient Monitoring and Assessment (GAMA) program (Belitz et al., 2003; Belitz et al., 2010) aims to assess the state and development of groundwater resources in California. A large proportion of the monitoring effort is dedicated to the collection and analysis of groundwater quality samples (Jurgens et al., 2010; Fram and Belitz, 2011; Landon et al., 2011; Deeds et al., 2012). Simultaneous collection and analysis of environmental tracers, including tritium, stable isotopes of the water molecule and dissolved noble gases and the helium isotope ratio, has created a large database containing valuable information regarding key groundwater characteristics, that allows assessment of contamination vulnerability and sustainability of groundwater abstraction.

This study aims to understand the vulnerability of the Mt Shasta area to drought and to differences in the timing of precipitation and runoff due to climate change. This study focused on three research questions:

1. What is the elevation of the source area for recharge to Mt Shasta groundwater systems?
2. What are the characteristics of groundwater flow paths?
3. What are the travel times from recharge to discharge locations?

We collected water samples from wells, springs, and surface water at a variety of locations and elevations. We analyzed the water for a suite of geochemical and isotopic tracers that can be applied to address questions related to recharge elevation, water-rock interaction and travel times. Some tracers are specific to a single research question, while others provide multiple lines of evidence for multiple questions. Samples were analyzed for the following geochemical and isotopic tracers: sulfur-35 (87.4 day half-life), sodium-22 (2.6 year half-life), tritium (12.3 year half-life), krypton-85 (10.8 year half-life), and carbon-14 (5,730 year half-life). Additionally, dissolved noble gases, general water chemistry (major anions and cations), and stable isotopes of water (δ^2H and $\delta^{18}O$) and carbon ($\delta^{13}C$) were measured to understand the sources of water and the chemical evolution of water along flow paths. Isotopic measurements are used to determine the apparent groundwater age over a broad age range, from less than one year to tens of thousands of years. Stable isotopes are used to determine the sources of water and the elevation of water sources. Dissolved noble gases allow calculation of recharge temperatures and can identify a mantle signature in the groundwater. General water chemistry enables examination of water source and water-rock interactions.

2 METHODS

2.1 Study Area

Mount Shasta is located in the southern portion of the Cascade Range geomorphic province, a region defined by volcanic activity. It is a compound stratovolcano 4,322 m in elevation located within Siskiyou County in northern California. Mount Shasta is composed of overlapping cones that developed over a period of over 100,000 years, the last eruption being in the 1700s. Mount Shasta's major lava flows consist of pyroxene-andesite lava flows, block-and-ash flows, and mudflows (Miller, 1980). Its high elevation creates a rain shadow effect on the northern and eastern portions of the mountain. This study focuses on the western side of the mountain.

The geology of Mount Shasta is characterized by Quaternary volcanics, primarily andesitic, basaltic, dacitic, and pyroclastic flow deposits (Wagner and Saucedo, 1987). Surrounding the peak of the mountain are Quaternary landslide deposits. North of the city of Weed, a town located west of the mountain, and on the southern flank of Mount Shasta are Quaternary glacial outwash and moraine deposits. Northeast of the mountain are extensive alluvial deposits. In addition, deposits of Ordovician partially-serpentinized Trinity peridotite are located on the western edges of Weed and Mount Shasta city, generally southwest of the mountain.

Mount Shasta is located in the Mediterranean climatic zone, which is distinguished by warm, wet winters and hot, dry summers with prevailing westerly winds, but the elevation of Mount Shasta creates distinct microclimates on its slopes (USDA, 2012). At elevations above 2,500 m, annual average snowfall is more than 2000 mm. The southwest side of Mount Shasta, near the city of McCloud, Mount Shasta and Weed, receives the most rainfall; the north side is semi-arid and windy and sparsely populated.

The California Department of Water Resources (California DWR, 2003) does not identify any groundwater basins in the region of Mount Shasta, and instead characterizes it as a groundwater source area. This excludes the area from regulation under the 2014 Sustainable Groundwater Management Act (State of California, 2014). Surface water runoff flows to the main drainages that form the Shasta, Pit, McCloud, and Sacramento Rivers. The nearby cities of Mount Shasta and Weed have an average annual precipitation of 99.4 and 60.1 cm, respectively (US Climate Data, 2015), with over 75% falling as snow between November and March.

In the study area quadrant (southwest portion of Mount Shasta), streams originating from snowmelt generally terminate at high elevation (above 3000 m), infiltrating into permeable surface materials. No major streams are present on the western side of the volcano. Sand of pyroclastic origin (tephra) that overlies basalt can exhibit high infiltration rates (Blodgett et al., 1988).

Volcanic flow deposits of varying compositions (both felsic and mafic) blanket the Mount Shasta region, making aquifer delineation a challenge. Basalts have significant pore space at the tops and bottoms of lava flows, resulting in a high porosity and permeability because of their relatively low viscosities and low densities after cooling. Basalts of Miocene age or younger, may contain water in "fractures, volcanic pipes, tuff beds, rubble zones, and interbedded sand layers..." (Planert and Williams, 1995). Columnar basalts may be developed in the center of flows, allowing water to move vertically. Unaltered pyroclastic rocks can have a porosity and permeability comparable to poorly sorted sediments, but altered pyroclastic material can become welded, resulting in an impermeable

deposit. Silicic lavas are very dense, with low permeability, unless fractured. In general, porosity and permeability decrease with depth in these volcanic formations. Tuffs or unfractured lava flows may cause confinement – the main production well in Mount Shasta City was free flowing (artesian) until about 1990.

2.2 Data Collection

We sampled water from springs, domestic and water supply wells, and streams in May and September 2015 – during a period of extreme drought (Table 1). Samples were collected from the City of Weed, located on the western portion of Mount Shasta; in the city of Mount Shasta, located southwest; and from wells and springs at higher elevations (Figure 1). All of the sampled springs are non-hydrothermal, or 'cold' springs. Additional snow samples were collected from the slopes of Mt Shasta between 1500m and 3100m elevation in February 2016.

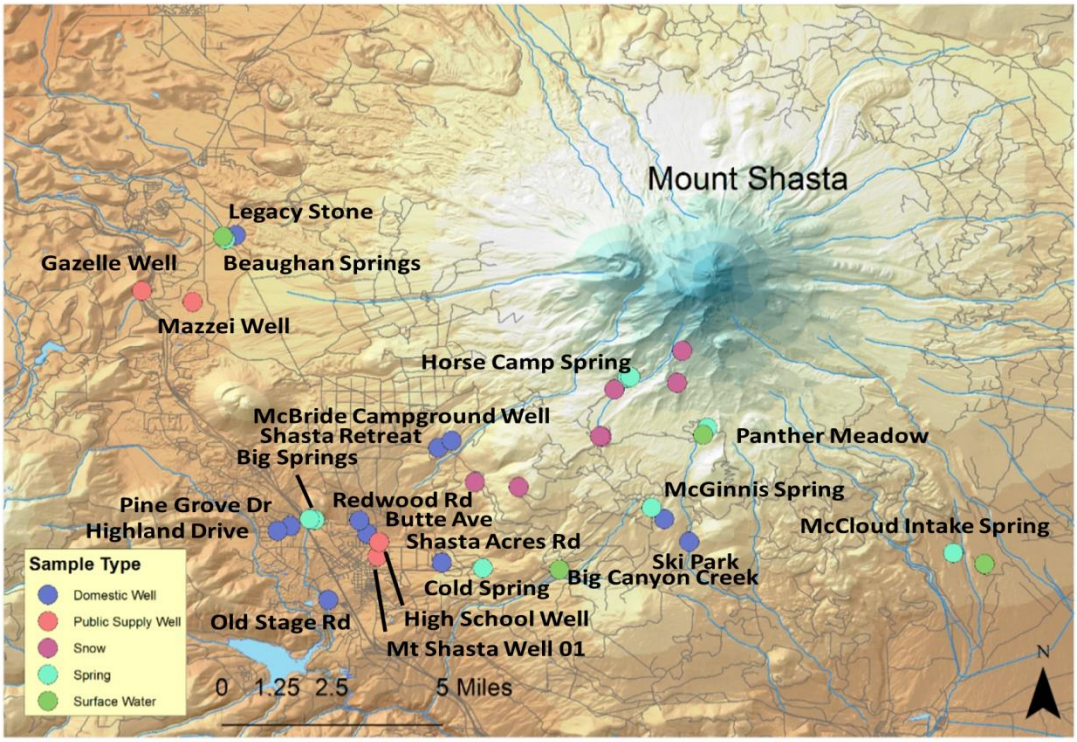

Figure 1: Location of water samples collected in May and September 2015, and of snow samples collected in February 2015. Sample sites are primarily located on the south western portion of Mount Shasta, except for the samples taken near the city of Weed and two samples taken near the McCloud River.

Samples were collected from the sample port of public supply wells or spigots of domestic wells. Samples for dissolved gases were collected carefully to avoid contamination by pressure tanks or the atmosphere. Water samples from springs were collected from tubing connected to an outflow port when one was available. Dissolved oxygen (DO), conductivity, temperature, pH, oxidation-reduction potential (ORP), and turbidity were measured at each location with a Thermo Orion Star A329 multi-meter.

Samples for tritium were contained in one liter glass Pyrex bottles, stable isotopes in 30 mL glass bottles, carbon-14 and carbon-13 in 40 mL volatile organic analysis (VOA) vials with zero headspace, general chemistry (anions and cations) in 125 mL plastic Nalgene bottles, and sulfur-35 in 20 L plastic carboys. Each aforementioned bottle was rinsed three times with water collected from the sampling port prior to sample collection. Sodium-22 samples were collected by passing 300L to 1000L of sampled water through a cation exchange resin column. A description of the sodium-22 sampling procedure is provided below. Noble gas samples were collected in pinch clamped copper tubes (Singleton and Moran, 2010). Krypton-85 samples were collected at 5 locations, in 20L air tanks by passing 2,000 – 4,000 L of water through a gas extraction system (Moran et al., 2008).

2.3 Sample Analysis

Samples were analyzed using a wide variety of laboratory methods. Cation and anion concentrations were analyzed by liquid chromatography (Metrohm model 881 Compact IC Pro). Stable isotopes of water were analyzed by isotope ratio mass spectrometry (IRMS, VG Prism; Epstein and Mayeda, 1953) and cavity ring-down spectroscopy (Los Gatos Research DLT-11 Liquid Water laser Isotope Analyzer). Tritium was analyzed by helium-3 accumulation (Clarke et al., 1976; Surano et al., 1992) and noble gas mass spectrometry (NGMS). Dissolved noble gas concentrations were measured by NGMS and noble gas membrane inlet mass spectrometry (NG-MIMS) (Visser et al., 2013). Carbon-13 was analyzed by IRMS (St-Jean, 2003; Singleton and Moran, 2010), carbon-14 by accelerator mass spectrometry. Sulfur-35 was analyzed by chemical precipitation of sulfate and liquid scintillation counting (LSC) (Uriostegui et al., 2015). Krypton-85 was analyzed by cryogenic purification and LSC (Visser et al., 2015; Alikhani et al., 2016). The procedure for sodium-22 was developed for this study and is described in detail below.

A new and straightforward analytical method was developed to determine sodium-22 activities from various water sources. In the field, 300L to 1000L of water are passed through a column containing 1.8 kg of cation exchange resin at a rate between 1 L/min and 10 L/min. Columns are returned to the laboratory where they are processed by passing 4L of 3M HCl through the resin columns to elute all cations. The 4L of acid is loaded into a Marinelli beaker for gamma ray spectroscopy analysis. The samples are counted for sodium-22 (1274 keV) using a coaxial germanium detector with a 0.5 keV resolution and a background of less than 3×10^{-3} counts per second. Samples are counted for seven days in order to acquire sufficient counts above background. The counting efficiency (11.6×10^{-3} cps/Bq) was obtained by counting a ^{22}Na standard of known activity in the same geometry and matrix (3M HCl in a 4 L Marinelli beaker) as the samples. The net peak area of the samples in a 2.5 keV window is compared to the net peak area of the standard to calculate the ^{22}Na activity.

2.4 Spatial Analysis

In support of the interpretation of the isotopic and chemical data, a spatial analysis was performed on publically available datasets of land cover (2011 National Land Cover Database; Homer et al., 2015), precipitation and temperature (PRISM Climate Group, Oregon State University, http://prism.oregonstate.edu) and vegetation index (MODIS NDVI Data, Spruce et al., 2016). The purpose of the spatial analysis was to constrain recharge rates and recharge source areas and compare elements of the water budget for the study area.

3 RESULTS AND DISCUSSION

3.1 Source Area

3.1.1 Stable Isotopes of Water

Stable isotopes of the water molecule ($\delta^{18}O$ and $\delta^{2}H$) are applied to identify water source, i.e., distance from an oceanic source, elevation, and latitude, as determined by position along the global meteoric water line and by comparison with extensive spatial data, and to detect post-depositional evaporation (as indicated by samples that fall on a lower slope than the slope of the global meteoric water line). The high elevation of Mt Shasta provides a large gradient in stable isotope signatures that are indicative of the source elevation of groundwater and springs. Previous work has established lapse rate of -2.3 ‰ per 1000 m increase in elevation (Nathenson et al, 2003; Rose et al., 1996). A wide range in $\delta^{18}O$ values is observed in samples from Mount Shasta (Figure 2, Table 2), owing to the very large elevation change from the base to the top of the mountain. Considering the elevation of the peak, an even greater range in $\delta^{18}O$ might be expected, with even lighter (more negative) values than those observed, if any of the samples had recharged entirely at near summit elevations. Figure 3 shows the $\delta^{18}O$ and $\delta^{2}H$ pairs, along with the global meteoric water line, and the close alignment of all samples to the line, indicating little variation in the source of moisture and no significant evaporation. Most groundwater well samples are located in the middle of the observed range for samples, possibly due to mixing of water sources in the aquifer.

Figure 4 is used to examine the relationship between $\delta^{18}O$ and the elevation of deposition. Results for snow samples collected at various elevations in February 2016 are in good agreement with the lapse rate. In the Mount Shasta setting, stable isotopes are therefore faithful indicators of the elevation at which precipitation (mainly snow), was deposited.

An important application of stable isotopes in this setting is to use them to identify the elevation at which water from springs or wells originated. Many spring and groundwater samples from approximately 1000-1400 m elevation have $\delta^{18}O$ values that fall well below the lapse rate trend line (Figure 4). This pattern indicates that groundwater from these locations is sourced from, and likely recharged at, much higher elevations. Considering the elevations indicated by the lapse rate, the water source elevations for all of the springs and wells sampled fall between approximately 2000 and 2900 m. Springs appear to recharge at somewhat higher elevations (2500m-2900m) than wells (2000m-2700m). The largest disparity between the sample elevation and the recharge elevation indicated by the $\delta^{18}O$ lapse rate is for Big Springs, where a difference of nearly 1700 m is indicated. In contrast, high elevation springs (Horse Camp 1 &2, Panther) show recharge elevations only slightly higher than sample elevations. Repeated samples from McBride Campground well (1483 m elevation) indicate a difference between recharge and sampling elevations of 750-1000 m, somewhat less than for most other wells and springs. It should be noted that the estimated $\delta^{18}O$ recharge elevation can be the result of a mixture of flow paths originating from a range of elevations. The absence of samples with estimated recharge elevations above 2900m or below 2000m is an indication that the $\delta^{18}O$ values could represent a mixture in which both higher and lower elevations are present. This interpretation is further discussed in the spatial analysis section below.

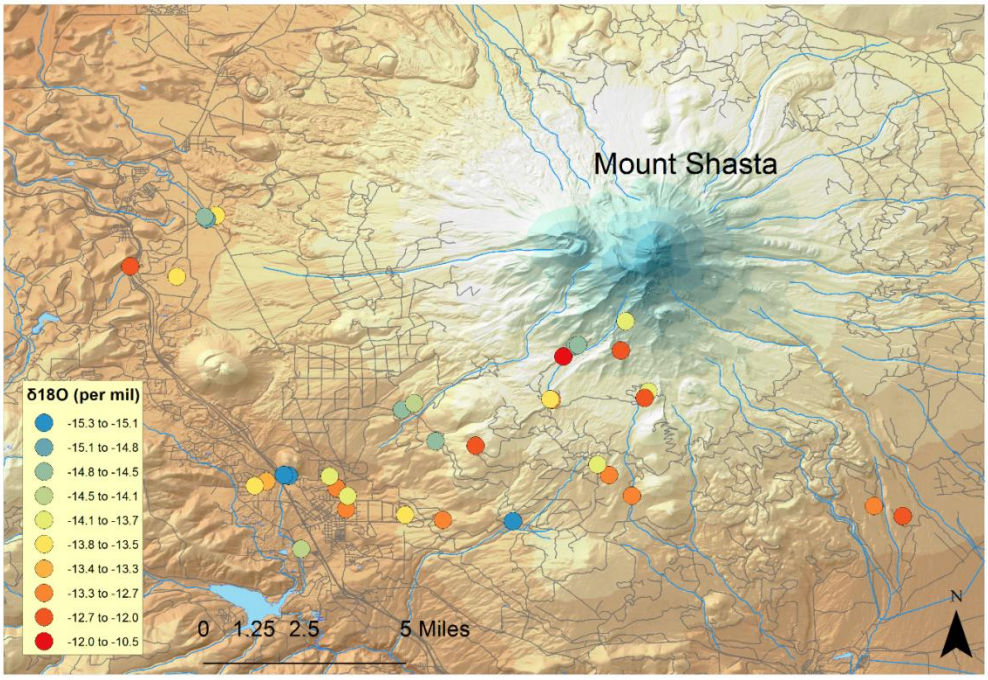

Figure 2: Spatial distribution of water isotopic composition Mount Shasta water samples – sample location symbols are color-coded by water oxygen isotopic composition ($\delta^{18}O$). More negative numbers (cooler colors) represent higher recharge elevations.

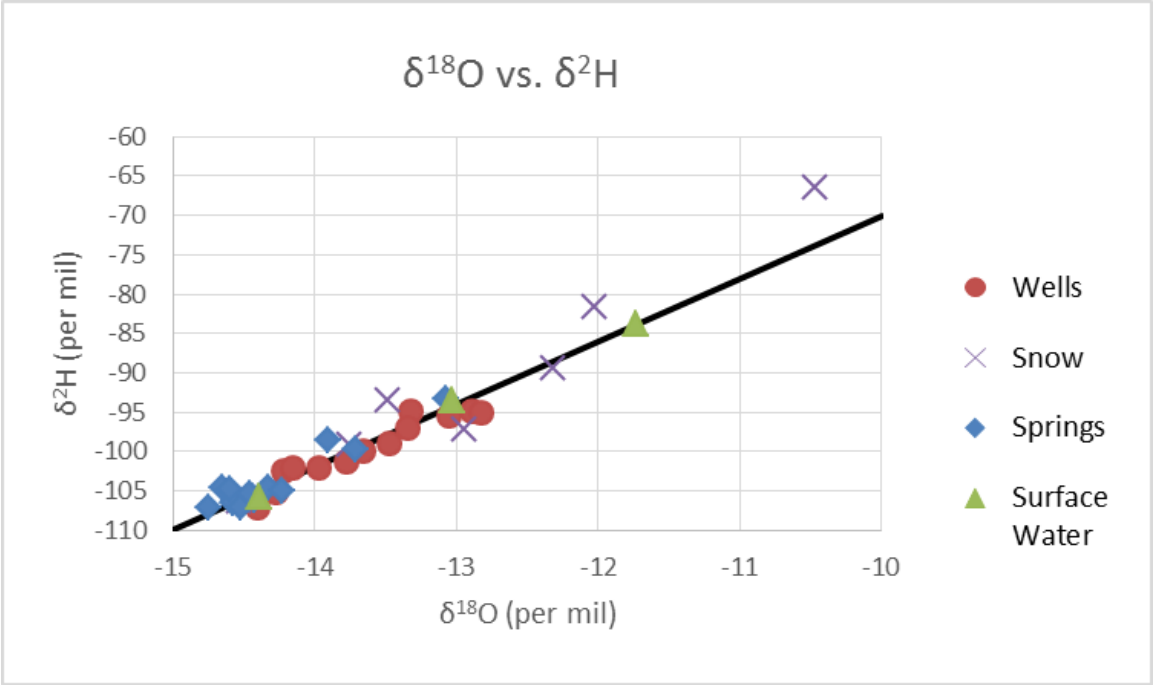

Figure 3: Water isotopic composition of samples from the Mount Shasta study region – hydrogen isotopic composition ($\delta^{2}H$) plotted against oxygen isotopic composition ($\delta^{18}O$) along with the global meteoric water line.

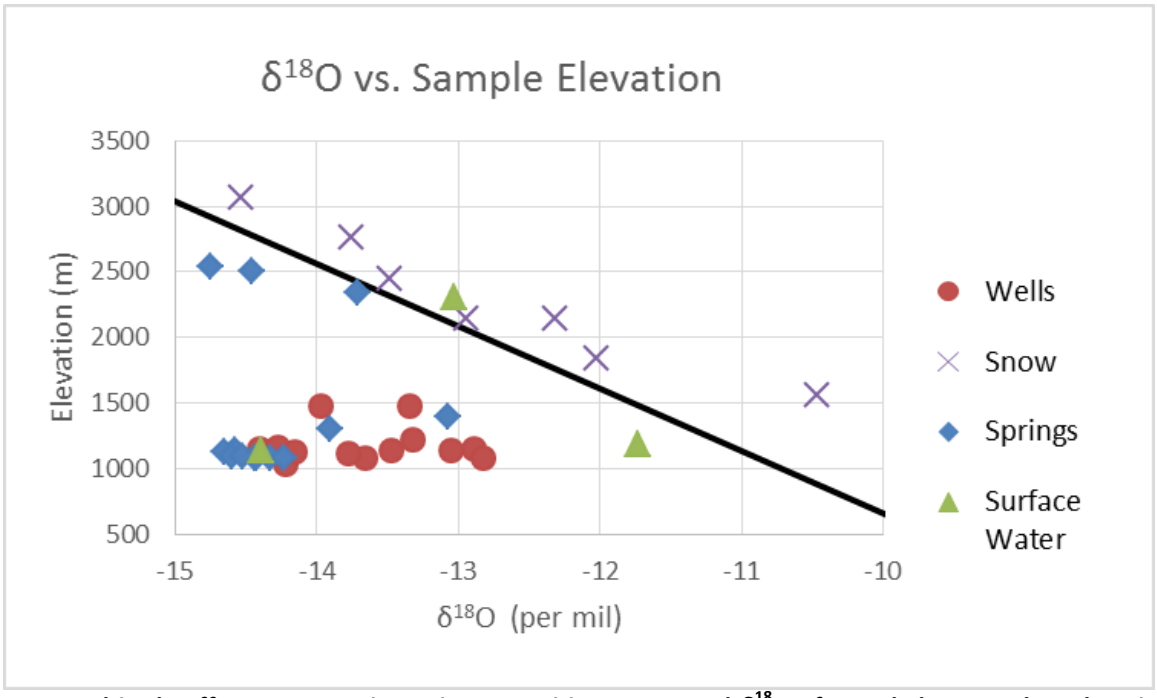

Figure 4: Altitude effect on water isotopic composition: measured $\delta^{18}O$ of sampled water plotted against sampling elevation for well, spring, surface water, and snow samples. Precipitation at higher elevation has a more negative $\delta^{18}O$ signature. The black line indicates a lapse rate of 2.3‰ decrease in $\delta^{18}O$ per 1000 m increase in elevation (Rose et al., 1996).

3.1.2 Noble Gas Recharge Temperature

Patterns in dissolved noble gas concentrations in groundwater samples (Table 3) provide an independent method for examining recharge elevations. The solubility of noble gases in water is a function of temperature, air pressure (controlled by altitude), and salinity (negligibly small in this study area). Because of their conservative behavior in groundwater, the concentration of noble gases, especially the heavier gases whose solubilities have a large temperature dependency, can be used to deduce groundwater recharge temperature. After measured noble gas concentrations are corrected for 'excess air' (Heaton and Vogel, 1981), recharge temperatures are calculated using an assumed pressure (or range of possible pressure/elevation) and equilibrium solubility relationships (Visser et al., 2016)

The maximum possible recharge elevation is the highest elevation on the mountain (4300m), while the minimum recharge elevation is the sample discharge elevation. Similarly, the minimum recharge temperature is 0°C, while the maximum recharge temperature is the discharge temperature. Under these limits, noble gas recharge temperatures were calculated at a range of elevations from the highest elevation possible on the mountain or lowest possible recharge temperature (0°C), to the lowest elevation or highest temperature (Table 4). The resulting ranges of possible recharge temperatures for each sample (represented as lines on Figure 5) have a slope equivalent to a 2 °C cooler recharge temperature per kilometer of elevation gain. Knowledge about the mean annual air temperature and atmospheric lapse rate then constrains the recharge elevation for these samples. The elevation at which the line for each sample intersects the atmospheric lapse rate line is a

plausible estimate of the recharge elevation. The probable recharge elevation of most wells lies between 2100 and 2900 m. Two wells (Highland Dr and Pine Grove Dr) are located on the west of the study area. Their chemical and radiogenic helium signatures indicate that they did not recharge on Mt Shasta and these two results are not included in the likely recharge elevation range.

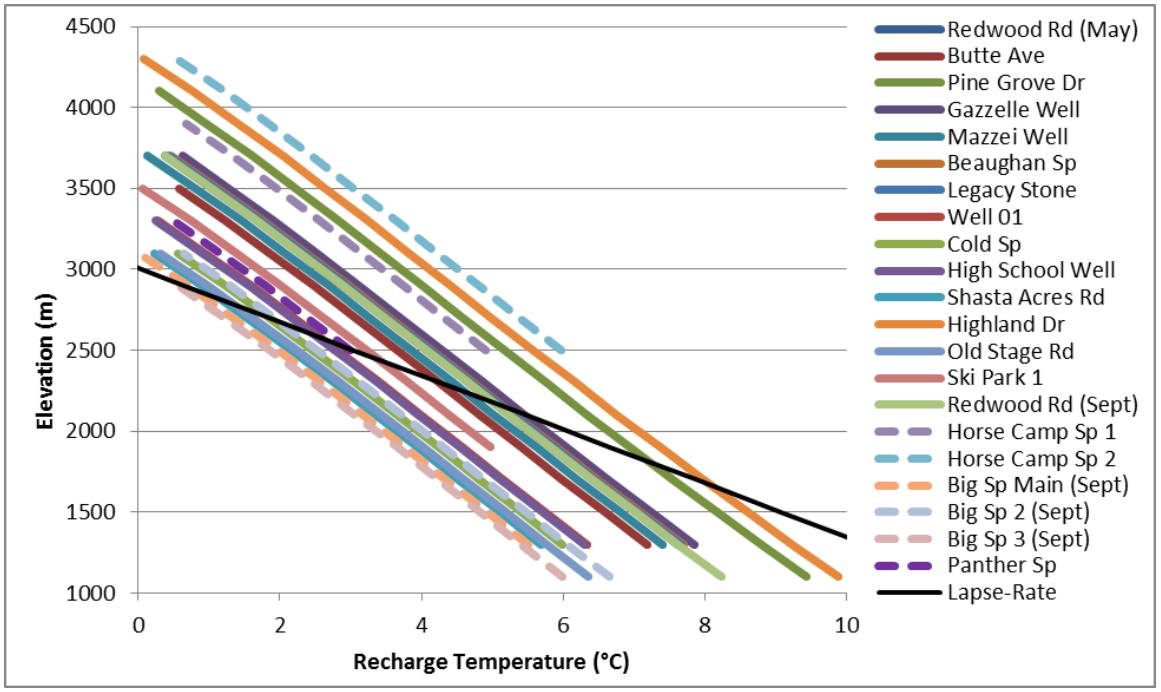

Figure 5: Noble gas recharge temperatures calculated at a range of elevations for each sample to include the range of P (elevation) and T combinations that are physically possible. The black line shows the expected atmospheric lapse rate (temperature as a function of elevation). Solid lines indicate copper-tube samples analyzed by the VG-5400 Noble Gas Mass Spectrometer and dashed lines indicate VOA-vial samples analyzed by the Noble Gas Membrane Inlet Mass Spectrometer.

The Big Spring samples which discharge at a low elevation (~1000 m), are located on the bottom left portion of the graph, indicating a lower recharge temperature than most other samples. Water from these samples likely recharged at a high elevation, meaning water feeding these springs has a relatively long residence time and long flow path. Other samples with similar recharge temperatures include Mazzei Well, Shasta Acres Rd, Old Stage Rd, and Highland Drive. These samples were taken from wells at low to mid elevations (1000 – 1300 m). Two sample lines don't intersect with the local lapse-rate - Horse Camp 1 and 2. It is possible these samples had a warm recharge temperature when the ambient air temperature was high (September). Alternatively, these samples may have been compromised during sampling.

3.1.3 Source Area Discussion

The two independent approaches to estimate the recharge elevation, $\delta^{18}O$ and fitting the noble gas recharge temperature to the atmospheric lapse rate, agree remarkably well for the majority of the samples (Figure 6). Since stable isotopes are indicators of water source but not necessarily recharge elevation, the good agreement also suggests that water is *not* generally transported long distances overland before recharging. This conclusion is corroborated by observed high infiltration rates in permeable surface materials and a lack of continuous creeks and streams in the study area. Two wells with noble gas recharge temperatures that indicate recharge below 2000 m (Pine Grove Dr

and Highland Dr) are located on the western edge of the study area and multiple lines of evidence (terrigenic helium, major ion and field chemistry) indicate this groundwater does not recharge on Mt Shasta. Three additional samples (Mazzei well, Beaughan Springs and Legacy Stone well) were sampled at the northern edge of the study area. For these wells, either the atmospheric lapse rate or the stable isotope trend could be different than the trend expected for the southwestern portion of Mount Shasta. The discrepancy for Shasta Acres Rd is unexplained. In summary, $\delta^{18}O$ and noble gases are in close agreement and both indicate that the range between 2000 m to 2900 m elevation is most important for recharge.

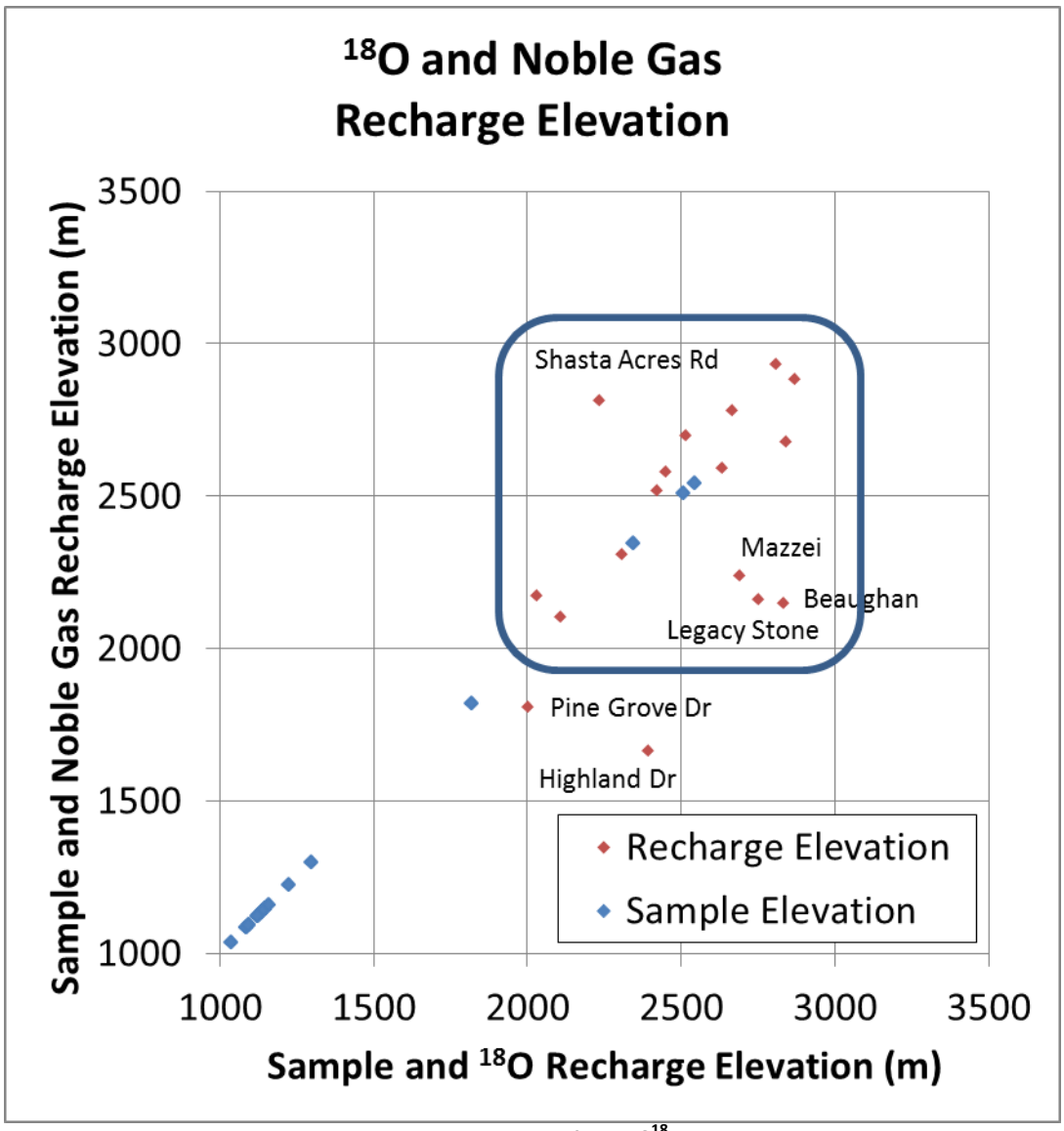

Figure 6: Sample and recharge elevation, determined from $\delta^{18}O$ and noble gas recharge temperature agreement with the atmospheric lapse rate.

3.2 Flow Paths

3.2.1 Temperature Changes between Recharge and Discharge

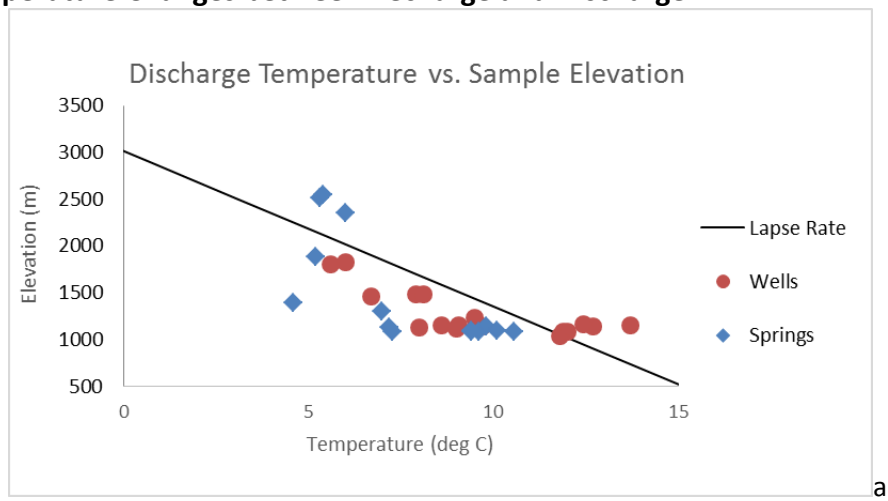

a

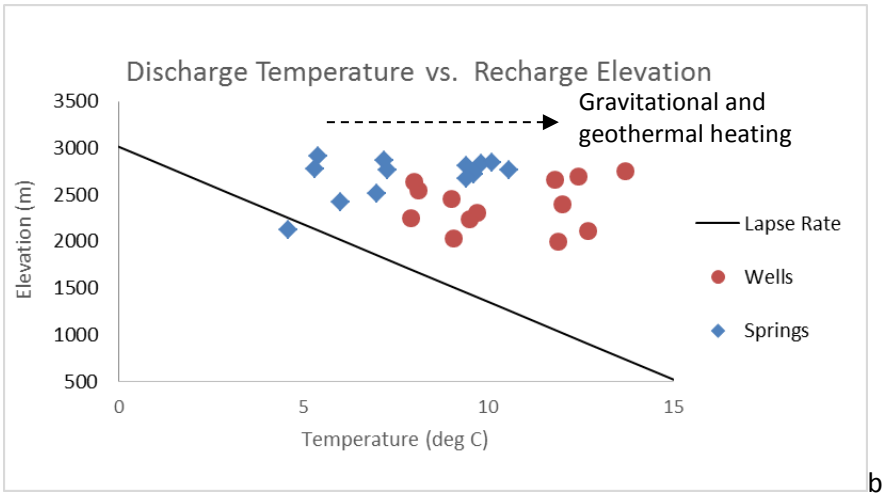

b

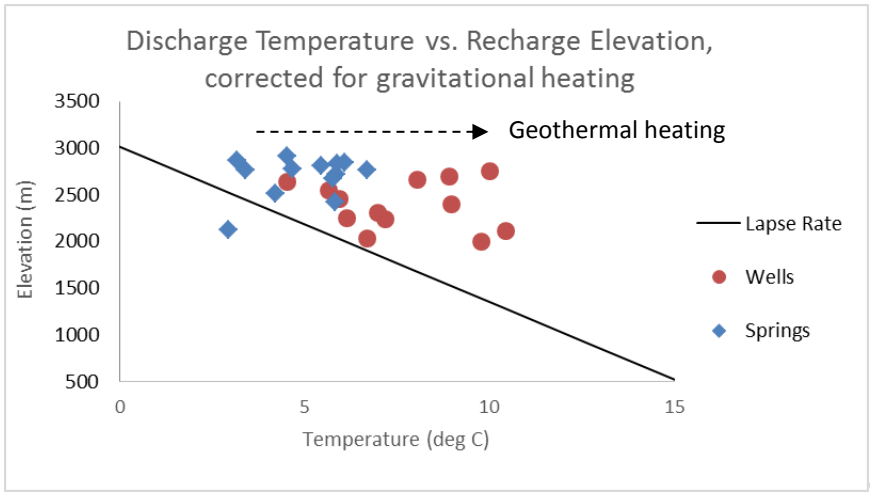

c

Figure 7. Discharge temperatures are plotted against sample elevation (a) and $\delta^{18}O$ recharge elevation (b). Discharge temperatures corrected for gravitational heating plotted against recharge elevation show the residual geothermal heating (c). Black lines shows the expected lapse rate of temperature vs. elevation.

Relationships between recharge temperature and discharge temperature contain information about groundwater flow paths. Discharge temperatures are plotted against elevation for wells and springs, along with the expected lapse rate of temperature vs. elevation in Figure 7a.

Most samples plot below the line, i.e., discharge temperatures are colder than the predicted ambient air temperature. Panther Spring, Horse Camp 1 and Horse Camp 2, which have discharge temperatures of 5-6 degrees C, were sampled in September in pools, so they were likely warmed due to the higher summer air temperatures. On the other hand, three wells that plot above the lapse rate at 13-14 degrees C may be influenced by deep flow paths and geothermal heating.

When discharge temperature is plotted against $\delta^{18}O$ recharge elevation (Figure 7b), nearly all samples plot well above the lapse rate trend, i.e., discharge temperatures are higher than recharge temperatures. Water moving through the subsurface transports heat and changes the subsurface temperature distribution. The rate of change of thermal energy in a parcel of groundwater is the sum of gravitational potential energy dissipation, heat transfer to/from the surface, and geothermal heating (Manga and Kirchner, 2004). In the case of Mount Shasta aquifers, conductive heat transport to/from the surface can be ignored because the advective rate of heat transport due to groundwater flow is likely much higher in the permeable aquifer materials. Using the elevation difference between recharge and discharge, as indicated by $\delta^{18}O$ and noble gas recharge temperature analysis, the potential energy dissipation (gravitational) term can be calculated and subtracted from the total energy change to reveal the geothermal heating component (Figure 7c). Figure 7c indicates that well samples, especially, show evidence for several degrees of geothermal heating during transport. The fact that well samples show greater geothermal heating than springs is likely due to deeper groundwater flow paths for at least a portion of the produced well water. Geothermal gradients are strongly affected by shallow groundwater circulation in the Cascade Range (Blackwell et al., 1990), with shallow gradients as low as 15 °C/km, but deeper gradients consistently >60 °C/km. For samples with 8 °C of geothermal heating and assuming a geothermal gradient at the low end of the observed range (15 °C/km), a maximum groundwater flow depth of about 500 m is indicated by this analysis.

Using the estimated recharge elevations, discharge locations, and maximum flow depths, groundwater flow paths for each sample can be delineated. Three example flow paths are shown on Figure 8 below. Recharge locations and flow depths are averaged and approximate; however, these flow paths are based on actual geochemical and isotopic observations and highlight the differences between the long, deep flow paths to the Mt. Shasta Big Springs and to wells on the lower slopes, and the short, shallow flow paths to smaller, higher springs.

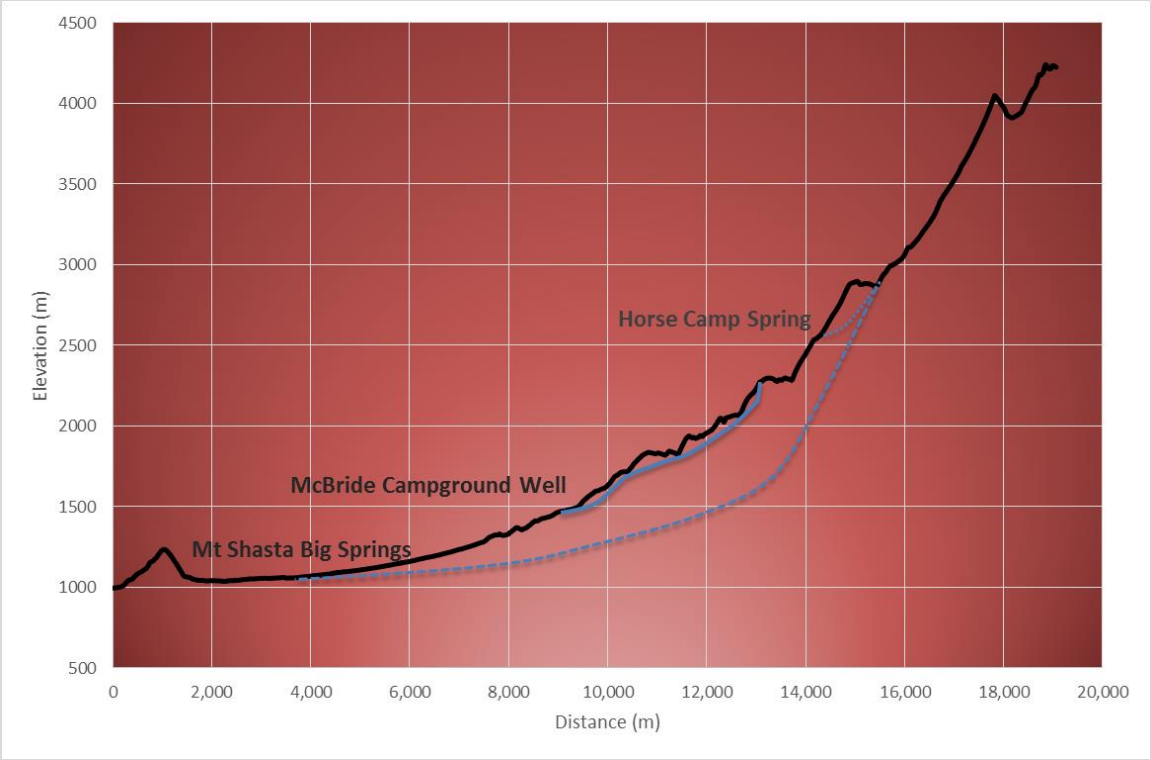

Figure 8: Example flow paths for three samples, drawn using calculated recharge elevations and maximum flow depths. Vertical exaggeration 4:1.

3.2.2 Field Parameters and Major Ions

Results for field parameters and major anions and cations are shown in Table 1 and 5. In general, samples from Mount Shasta have very low dissolved solids contents, pH values somewhat more acidic than neutral, high dissolved oxygen concentrations, and near zero Eh potential. Samples from higher elevations have lower electrical conductivity (Figure 9), though low elevation samples from just above 1000 m exhibit a wide range in conductivity, possibly because samples from lower elevations have had more time for water-rock interaction. Springs located at high elevations, such as Horse Camp 1, Horse Camp 2, and Panther Spring have the lowest ion concentrations.

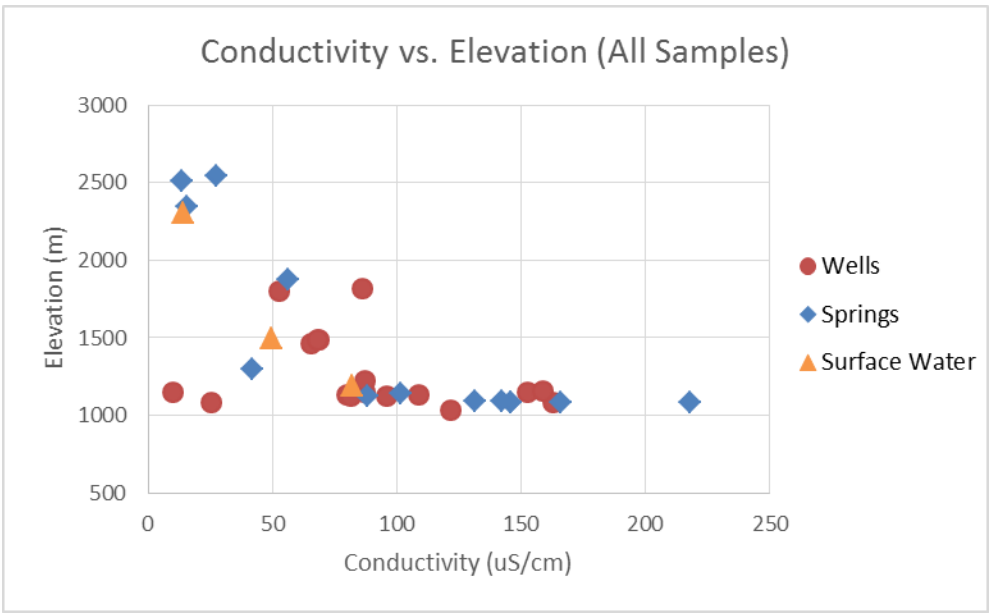

Figure 9: Conductivity plotted against elevation for wells, springs, and surface water in the Mount Shasta region.

A piper plot (Figure 10) sheds light on the chemical composition of sampled waters and water-rock interactions along groundwater flow paths. The anion composition is most distinct, revealing three chemical signatures (Figure 11):

- Sulfate dominated, found at Legacy Stone and Beaughan Springs, west of Mt Shasta in the northern portion of the study area
- Chloride dominated, found at Pine Grove Dr and Highland Dr, southwest of Mt Shasta, on the west side of the study area
- Bicarbonate dominated, found at Mt Shasta Cold Spring and wells in the City of Mt Shasta, on the south side of the study area.

The cation composition is less useful for distinguishing groupings. Snow and Panther Meadow Creek are dominated by sodium and potassium, which varies between 20% and 40% in the wells and springs. Magnesium contributes less than 20% to the cation charge in all samples. Calcium contributes between 40% and 80% of cation charge and is the most prominent manifestation of water-rock interaction.

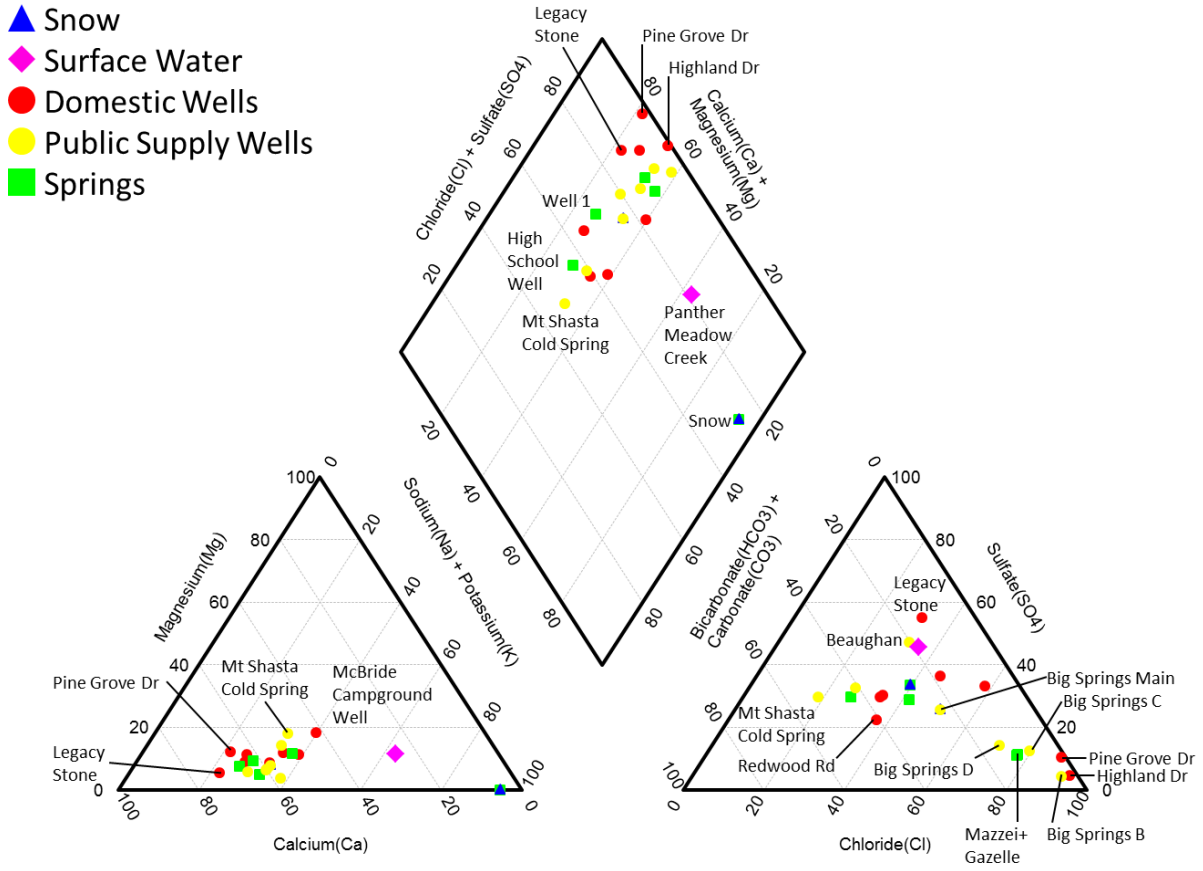

Figure 10: Percent contributions of cation (magnesium, sodium + potassium and calcium) and anion (chloride + fluoride, bicarbonate and sulfate) concentrations to the charge balance, in Mount Shasta well, spring, and surface water samples.

The anion composition is mapped in Figure 11, with the inset figure serving as color legend. The two main spring systems in Mt Shasta (Big Springs and Cold Spring) show distinct chemical signatures. Big Springs' chloride signature (dark red in Figure 11 map and inset diagram) resembles that of the wells that are in the western part of the study area (bright red in Figure 11). This chloride signature is close to the signature of the bicarbonate waters (blue in Figure 11) in Cold Spring and wells on the southeastern part of the study area. North of Mt Shasta City, Beaughan Springs and Legacy Stone well show a sulfate signature (green), distinct from the chloride signature that is found in the nearby Mazzei and Gazelle wells.

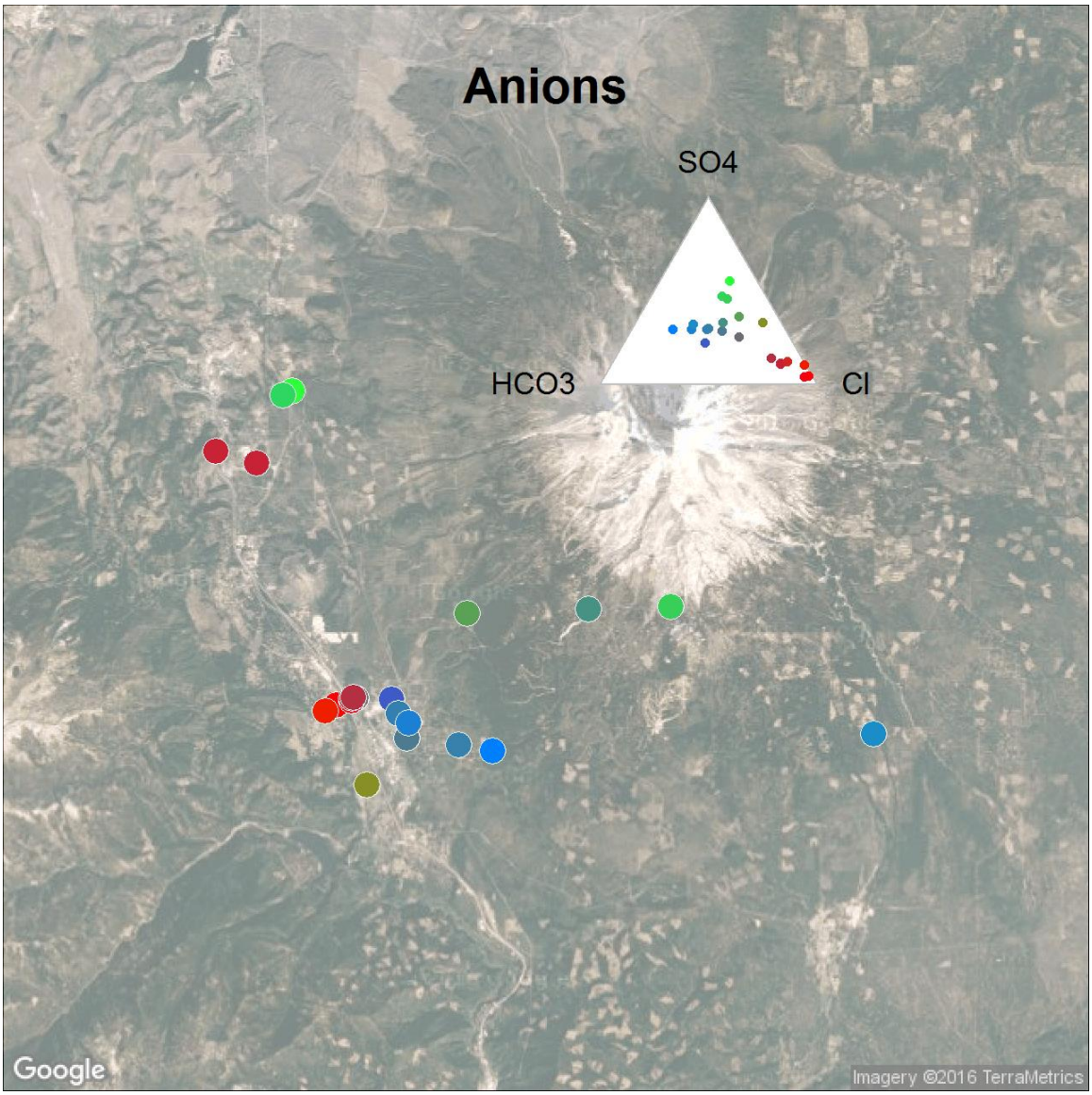

Figure 11: Map of sampled well locations. Colors represent anion chemistry. Colors in inset figure provide legend for mapped locations. Inset figure is the bottom-right diagram of piper plot (Figure 10).

Linear trends are likewise evident between concentrations of individual ion pairs (Figure 12), suggesting mixtures between sources and showing generally higher concentrations in wells than in surface water and springs. Previous authors (Blodgett et al., 1988) observed higher monovalent ion (Cl- and K+) concentrations in waters drawn from andesite flows. Mixtures between these waters and water hosted by basaltic flows may explain the linear mixing trends. Longer times for water-rock interaction are also a likely explanation for the observed ion patterns, and are discussed further below.

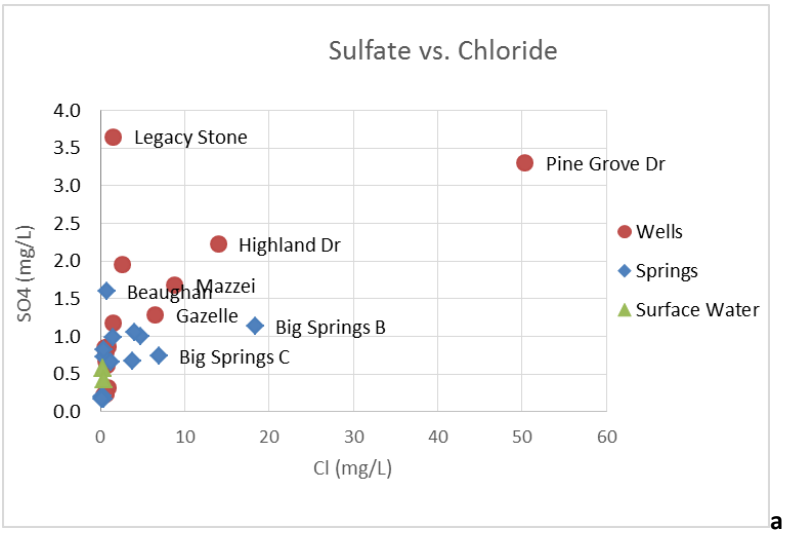

a

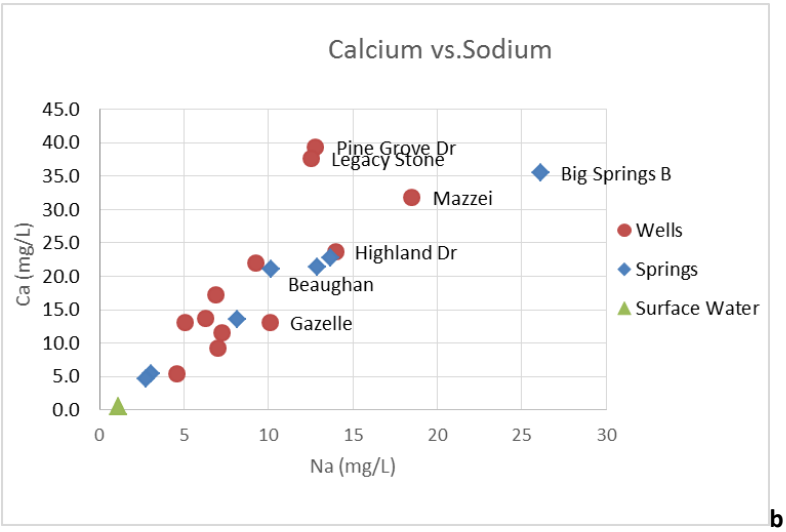

b

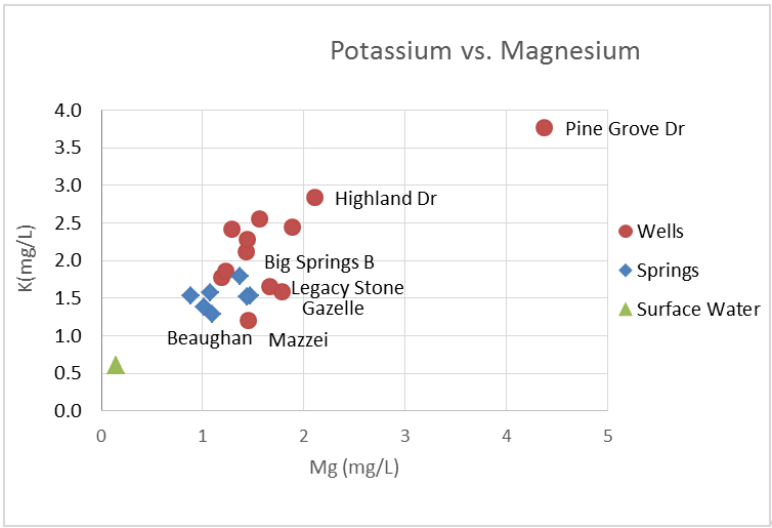

c

Figure 12: Sulfate (SO_4) plotted against chloride (Cl) (a), calcium (Ca) plotted against sodium (Na) (b) and potassium (K) plotted against magnesium (Mg) (c) for wells, springs, and surface water in the Mount Shasta region.

3.2.3 Dissolved Inorganic Carbon and Carbon Isotopes

Stable and radioactive isotopes of carbon, along with dissolved inorganic carbon (TIC) concentrations reveal additional information about groundwater flowpaths and subsurface residence times. Results for TIC and carbon isotopes ($\delta^{13}C$) are shown on Table 6. TIC increases in the subsurface due to CO_2 production by biologic activity in soils (organic matter has variable $\delta^{13}C$ but is typically near -25‰), remineralization of organic C, and dissolution of carbonates ($\delta^{13}C$ = 0‰). Dissolved CO_2 that evolves from atmospheric CO_2 by addition of soil CO_2 from plant respiration and some carbonate dissolution in an open system reaches an equilibrium $\delta^{13}C$ of about -16‰ at the water table. Figure 13 is a mixing diagram, with inverse TIC concentrations plotted against the stable carbon isotope ratio. Expected end member compositions are identified and mixing relationships between end members are inferred. Horse Camp 1, Horse Camp 2, and Panther Spring have very low TIC concentrations and the Horse Camp springs have $\delta^{13}C$ values near the expected atmospheric CO_2 value of -7.7‰. The trend showing the evolution of $\delta^{13}C$ in TIC from the atmospheric to the soil endmember with increasing TIC is exemplified by a mixing line that originates at Horse Camp Spring and evolves through Ski Park well, Shasta Retreat well, and Gazelle well toward a $\delta^{13}C$ of -16‰ (Figure 13).

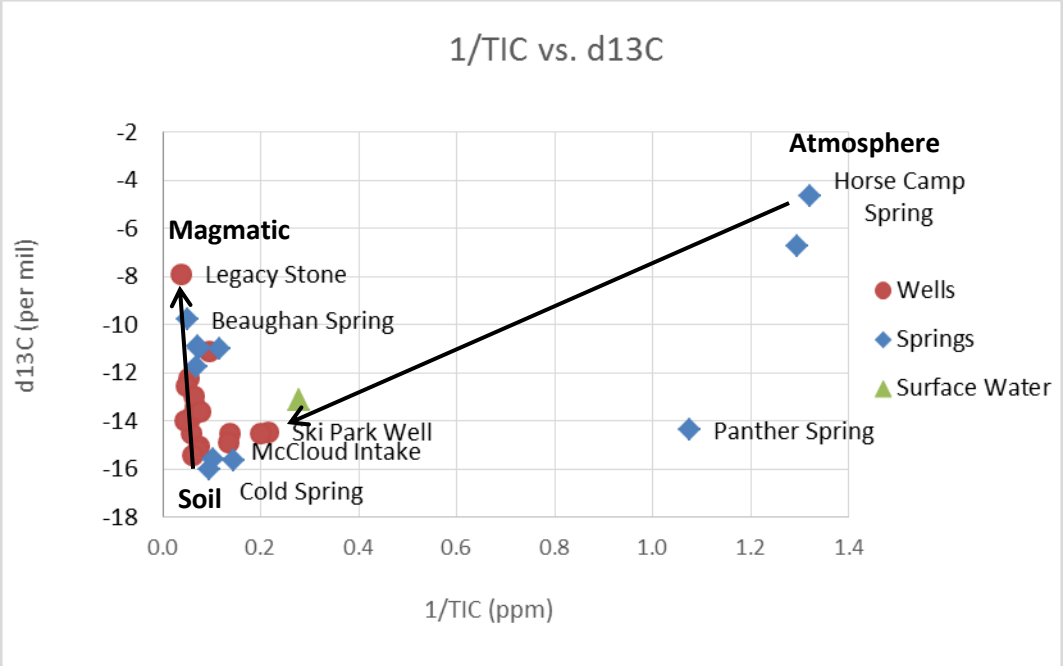

Figure 13: Total inorganic carbon (TIC) plotted against $\delta^{13}C$ for Mount Shasta wells, springs, and surface waters. The right downward trending arrow shows the expected evolution of water in equilibrium with air to a "soil endmember" in which water is in equilibrium with soil gas. The left upward trending arrow shows the evolution of a soil endmember water with the addition of mantle CO_2.

Another trend is also apparent, between the soil end member, with $\delta^{13}C$ of -16‰ (bottom left), and a magmatic CO_2 end member with higher TIC and a $\delta^{13}C$ of approximately -8‰. The two samples that show the addition of magmatic CO_2 are the Legacy Stone Property well and Beaughan Spring. These samples are located adjacent to each other in the northwestern portion of the study area. Most samples collected in this study plot along the soil-to-magmatic trend, meaning that recharge took place through a soil with some biological activity adding CO_2, followed by addition of CO_2 with a magmatic signature (Rose et al, 1996).

Samples with an atmospheric ^{13}C signature and low TIC are rare. Such a signature can develop by recharge through a land surface of bare rock. The absence of samples with this signature indicates that recharge exclusively above the tree line (2500 m) does not contribute significantly to the spring and well waters sampled..

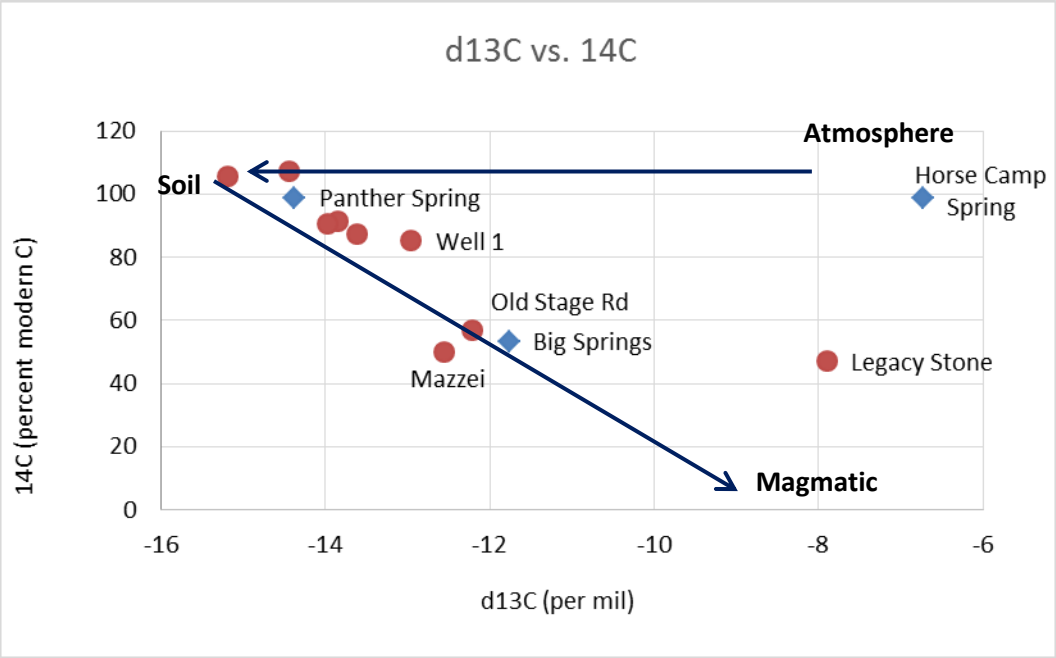

Figure 14: $\delta^{13}C$ plotted against carbon-14 for Mount Shasta wells and springs.

^{14}C and $\delta\ ^{13}C$ are combined in Figure 14, which also shows the approximate fields for a magmatic endmember ($\delta^{13}C$ of -8‰, 0 ^{14}C pmC), soil CO_2 endmember ($\delta^{13}C$ of -16‰, 100 ^{14}C pmC), and atmospheric endmember ($\delta^{13}C$ -7.7‰, 100 ^{14}C pmC). Most of the samples analyzed fall along a linear trend between soil and magmatic end members, in agreement with the results shown in Figure 13. In this view, McBride Campground, Ski Park Well 1, and Panther Spring fall close to the soil end member, where recharge through a forested soil, but little additional alteration of the inorganic carbon is indicated. Other wells and Mount Shasta Big Springs show an evolution in TIC and possible addition of magmatic CO_2.

3.2.4 Helium Isotopes

As noted above, tritium-helium dating is generally precluded in areas of significant volcanic activity because even small contributions of magmatic fluids drastically alter the $^{3}He/^{4}He$ ratio, making quantification of tritiogenic ^{3}He, used in tritium-helium dating, impossible. Tritiogenic, atmospheric, radiogenic, and mantle helium trends are plotted on Figure 15 to understand the helium sources in the samples (Welhan et al., 1988). Five samples have a strong magmatic/mantle signature (falling along the purple line that intersects the vertical axis at the established $^{3}He/^{4}He$ ratio for magmatic fluids of 8 times the atmospheric ratio), including Well 01, Old Stage Rd, Mazzei Well, High School Well, and Shasta Acres Rd. Three samples have a significant radiogenic component. Two of these (Pine Grove Drive and Highland Drive) were collected on the western edge of the City of Mt Shasta and are not likely part of the same flow system as the other samples. Radiogenic (Figure 16, blue symbols) and mantle (Figure 16, red symbols) helium isotope signatures are present in Mt Shasta groundwater in close proximity.

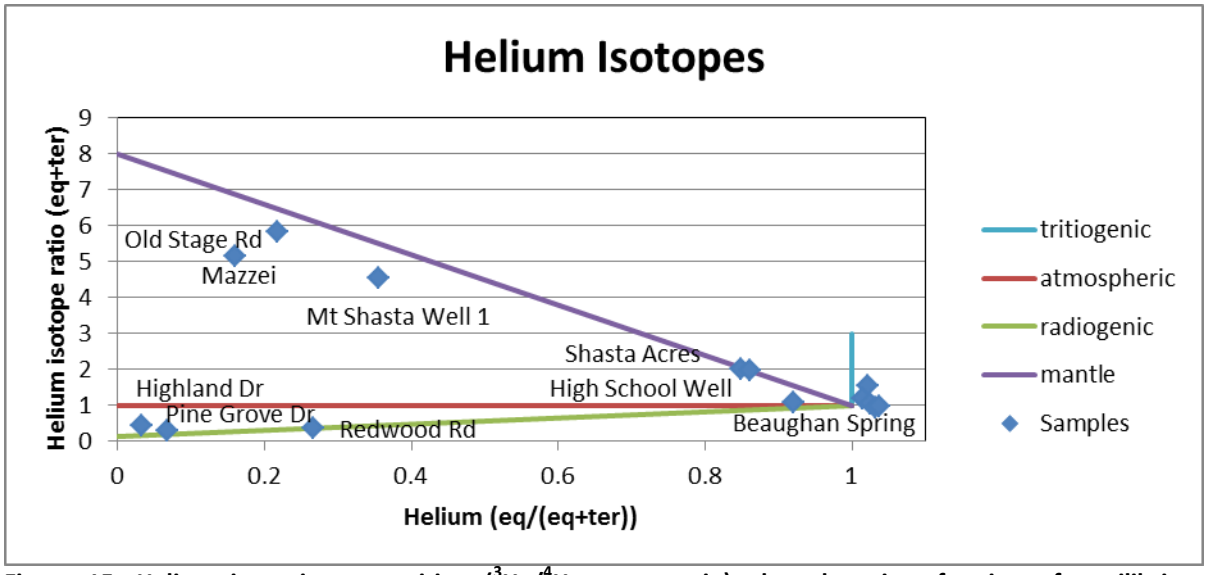

Figure 15: Helium isotopic composition ($^{3}He/^{4}He$ atom ratio) plotted against fraction of equilibrium atmospheric helium to total helium (after correction for excess air). Trend lines are shown for the addition of tritiogenic, atmospheric, radiogenic and mantle helium to equilibrium atmospheric helium.

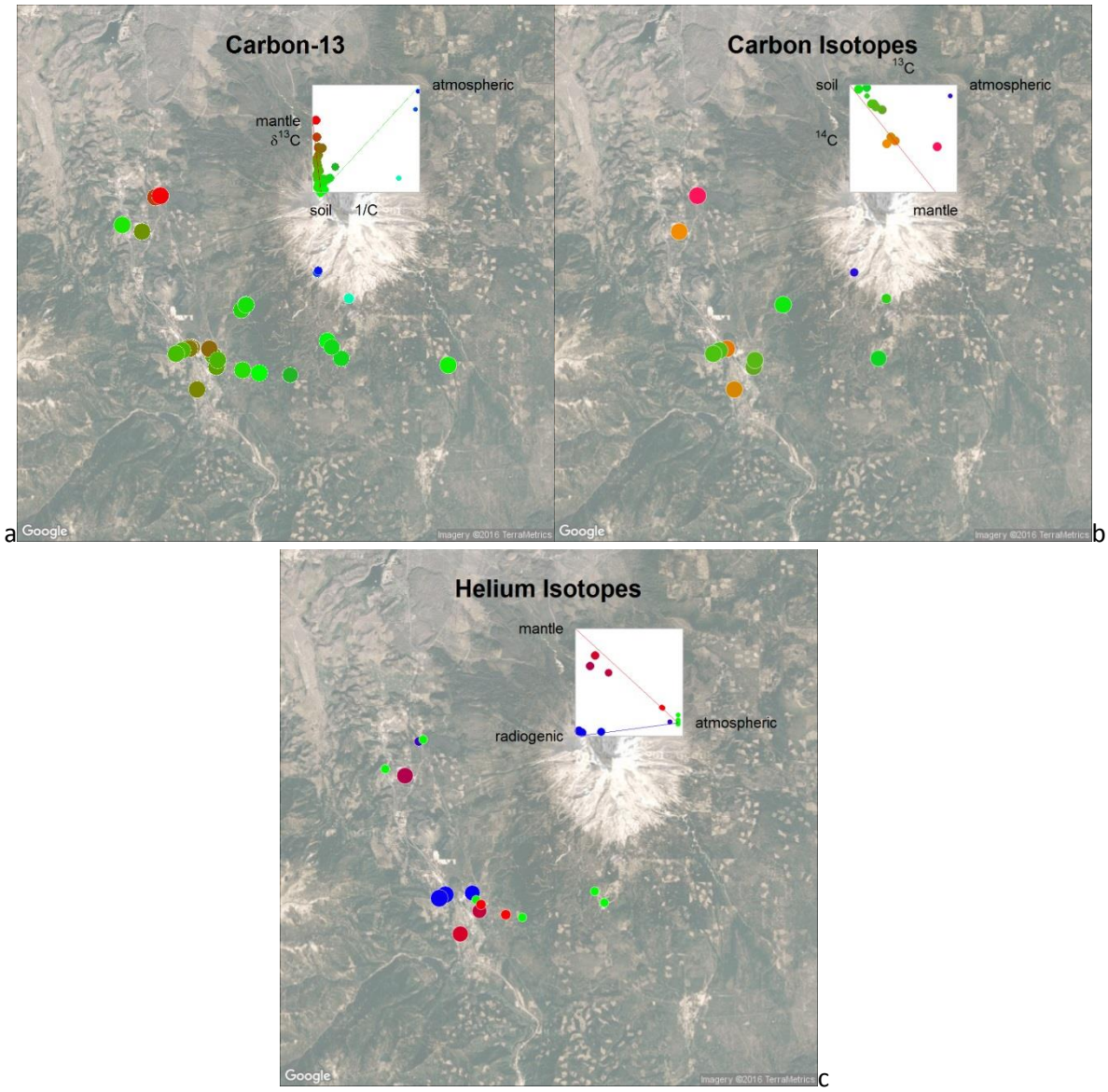

Figure 16: Maps of carbon-13 and dissolved carbon (a), carbon isotopes ^{13}C and ^{14}C (b), and terrigenic helium isotopic composition (c) in sampled groundwater wells at Mt Shasta. Although not all samples were analyzed for each analyte, both carbon and helium isotopes show mantle derived fluids. Inset figures serve as color scales for mapped locations and are reproductions of Figures 13, 14 and 15.

3.3 Travel Times

Several radiometric groundwater age tracers were analyzed in order to examine groundwater residence times, using isotopes with a wide range of half-lives, ranging from 87 days (^{35}S) and 2.6 years (^{22}Na) to 10.8 years (^{85}Kr) and 12.3 years (^{3}H). ^{35}S, ^{22}Na and ^{85}Kr were analyzed at a limited number of sample locations, due to the large volume of sample required to produce a reliable result. Additional "old" tracers (^{4}He and ^{14}C) were analyzed but their interpretation was complicated by geogenic sources of these isotopes, as discussed before.

3.3.1 Sulfur-35

Sulfur-35 was detected in replicate snow samples collected at 2140 m elevation in May, at a level of 3.1±0.9 mBq/L (Table 7). This value was assumed to represent the average snow input for that season. Sulfur-35 was also detected in Panther Meadow Creek, at 2.2±0.7 mBq/L, representing 70% recent snow. Sulfur-35 was not detected in any of the other samples collected at Mt Shasta. Considering the (95% confidence limit) detection limit of less than 1 mBq/L for these samples, the contribution of recent snow was less than 30% for all sampled wells and springs indicating that the bulk of the sampled water has a subsurface residence time of more than about 18 months. Sulfur-35 was detected in the main Big Springs outlet in September 2015, at 0.7±0.4 mBq/L (detection limit: 0.5 mBq/L). This is evidence that a fraction of water discharging from Big Springs had recharged very recently. This fraction cannot be quantified accurately, because no precipitation was sampled between May and September. Sulfur-35 activities in summer precipitation have been observed to be orders of magnitude higher than in winter precipitation. This could also point to delayed arrival of recent precipitation at the main Big Springs outlet. This uncertainty prohibits the quantification of the recent precipitation contribution at Big Springs.

3.3.2 Sodium-22

Six sodium-22 samples were processed at Mt Shasta (Table 8). The volume of water processed varied between 0.29 m^3 (Big Springs) and 1.0 m^3 (High School Well). As a result, the detection limit varied from 34 mBq/m^3 to 10 mBq/m^3. No snow sample was processed at Mt Shasta, but two entire-season snow samples were collected at the Southern Sierra Critical Zone Observatory (SSCZO) representing the winter precipitation of 2014-2015 and 2015-2016. The measured activity in SSCZO snow was 141±35 mBq/m^3 and 153±29 mBq/m^3, respectively. Considering the 2014-2015 SSCZO snow activity, the detection limits achieved for the Mt Shasta samples correspond to between 7% and 24% of recent snow. These results are in agreement with the sulfur-35 results. Sodium-22 results indicate that the travel time of sampled wells is longer than 5-10 years. Sodium-22 relies on less well-constrained initial activity and is therefore less precise.

3.3.3 Tritium

Unlike the shorter-lived isotopes, tritium (half-life 12.3 years) was detected in all but two samples from Mount Shasta (Table 9). Nearly all samples therefore show evidence for at least a component of water with a residence time of less than 50 years. Tritium activity is affected by both spatial patterns in precipitation (with higher values expected for higher elevations (Harms et al., 2016)), and by the decay of tritium during groundwater flow. Samples from higher elevations on Mount Shasta do generally show a higher tritium activity (red colors; Figure 17). Also, higher tritium activities are correlated with lower electrical conductivity (as measured by a field probe). This pattern is likely due to the fact that with increasing subsurface residence time, water has more time to interact with bedrock and soil, which contributes to increasing conductivity. Activities in lower elevation samples are lower and show more variability, due to the decay of tritium over time scales of several decades.

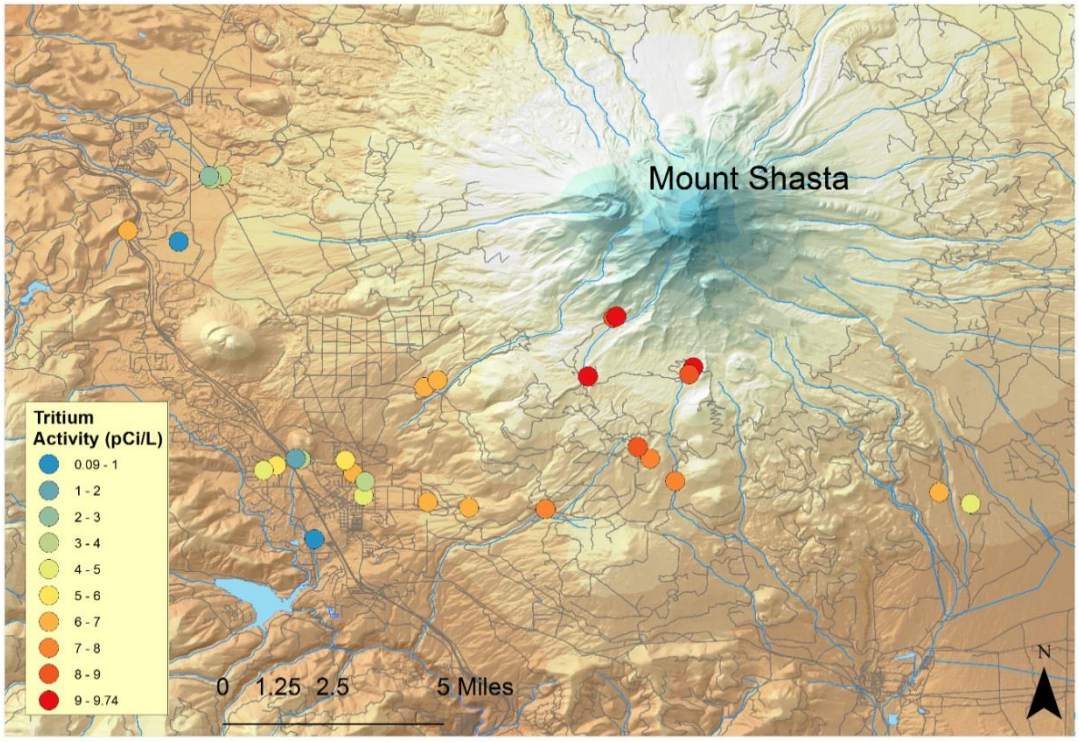

Figure 17: Spatial distribution of tritium activity in Mount Shasta water samples – sample location symbols are color-coded by tritium activity.

3.3.4 Krypton-85, Tritium and Tritium/Helium-3 Groundwater Ages

Tritium-helium age dating is challenging in volcanic environments because of the potential for widespread influx of magmatic fluids, which drastically affect the He isotope ratio, and preclude accurate tritium-helium age dating. For that reason, ^{85}Kr, with a half-life of 10.8 years, was also analyzed, since it is not affected by magmatic fluids, but rather only by steadily increasing atmospheric ^{85}Kr activities resulting from the global re-distribution of ^{85}Kr released to the atmosphere by nuclear fuel reprocessing. Five wells were sampled for ^{85}Kr, which requires passing a large volume (0.5-1 m^3) of groundwater though membrane contactors (Table 10). Figure 18 shows analytical results for ^{85}Kr and tritium (expressed as percent initial ^{3}H activity as determined from a Bunny Flat snow sample), along with a (red) line showing reconstructed values in precipitation (tritium) and the atmosphere (krypton-85) back to 1950.

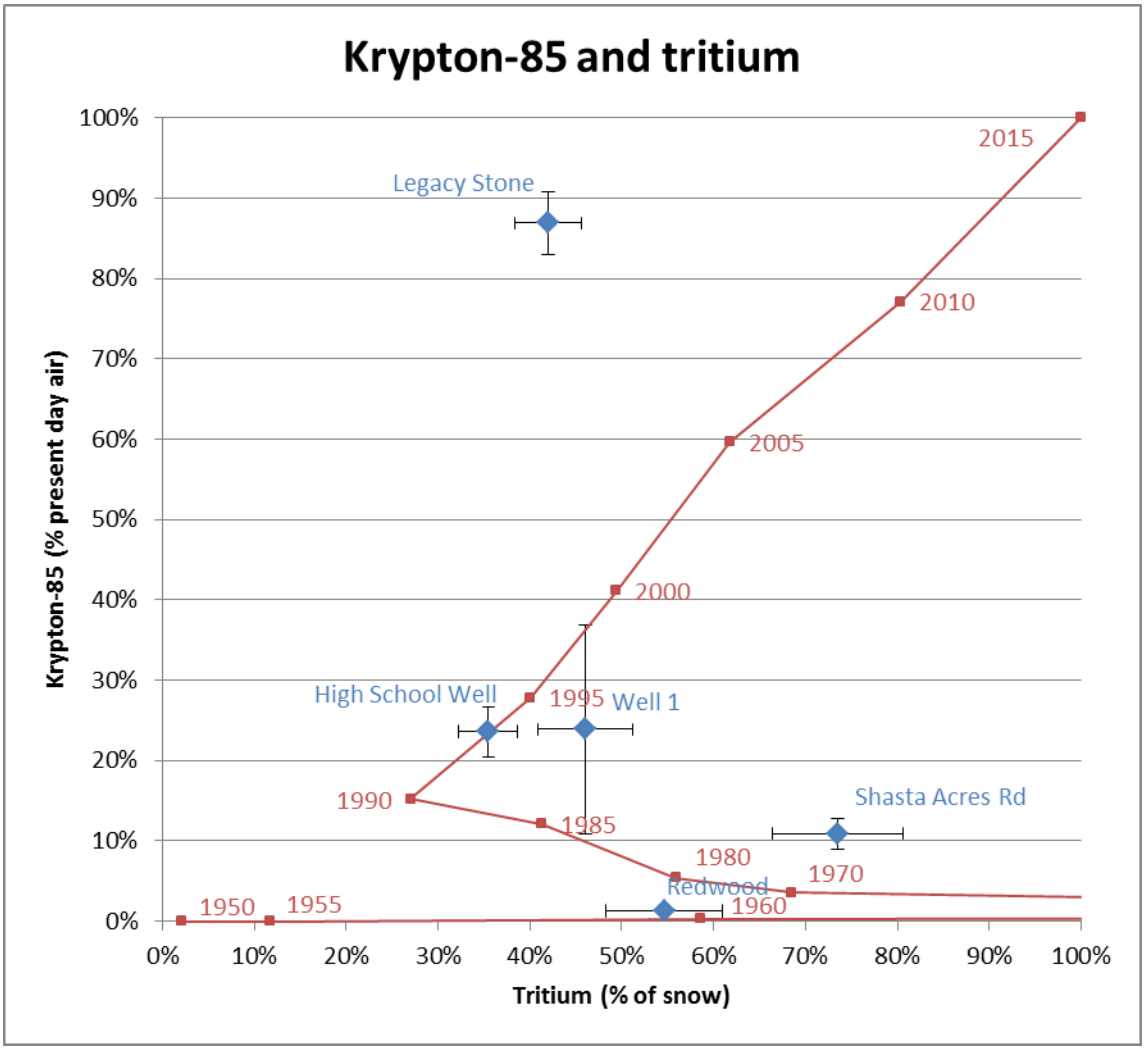

Figure 18: Tritium (expressed as percent of initial (snow) concentration) and krypton-85 (expressed as percent of present day air) results are plotted along with a (red) line showing reconstructed values in precipitation (tritium) and the atmosphere (krypton-85) back to 1950.

Three of the samples plot close to the line, making their ages clear: High School Well (~1994), Shasta Acres Rd (~1970), and Redwood Road well (~1959). Well 1 has a large krypton-85 error, so it may have an age of about 1984 or 1998, a 14 year difference. Legacy Stone well is located far from the line and has a relatively small error, indicating this sample was likely contaminated by present-day atmospheric krypton-85 during sampling. The krypton-85 results confirm that most sampled groundwater has mean subsurface residence times of over 10 years or more. The result for Shasta Acres Rd points to a mixture in which a small contribution of bomb-derived tritium results in a higher tritium activity than can be the result from decay of present-day tritium levels, suggesting the ^{85}Kr result of ~1984 is more appropriate.

For two wells, a reliable $^{3}H/^{3}He$ age could be calculated: Gazelle Well (22±2 years) and Butte Ave (35±2 years).

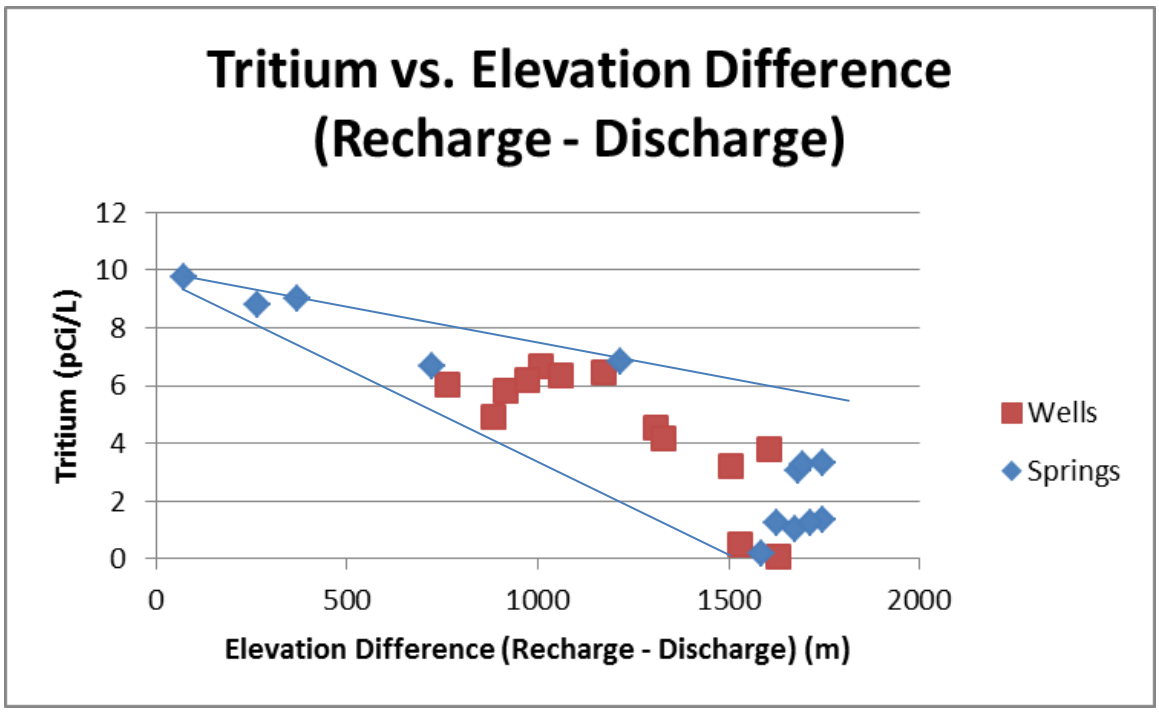

Figure 19: Measured tritium activity plotted against the difference between recharge elevation (estimated from stable isotopes) and discharge elevation in the upper plot and against groundwater flow distance in the lower plot shows the decay of tritium during flow down the slope of Mt Shasta.

A plot of tritium concentrations vs the elevation lost between recharge (based on $\delta^{18}O$) and discharge (Figure 20) shows a trend from an initial concentration in precipitation of 9-10 pCi/L, down to 0-3 pCi/L after an elevation loss of over 1700 m. The narrow range around the slope suggests that tritium is a reasonable qualitative age indicator for many of these samples, especially high elevation springs that are not subject to significant mixing.

3.3.5 Discussion of Groundwater Travel Times at Mt Shasta

Water supply wells of the City of Mt Shasta (Well 01 and High School Well) produce water with an age of 15-20 years, based on tritium and krypton-85 analyses (Table 11). Cold Spring discharges younger water. Based on sulfur-35 and sodium-22, the fraction of water with an age less than 1 year in Cold Spring is at most 25%. The tritium model age is 5 years. Sodium-22 was not detected resulting in a model age of more than 7 years. However, ^{22}Na relies on less well-constrained initial activity and is therefore less reliable.

The water supply wells for the City of Weed produce water that is mixed age (Gazelle with an average of 20 years) or is pre-modern (Mazzei). The very low tritium activity in the Mazzei well means that the well delivers almost entirely pre-modern groundwater.
Domestic wells in Mt Shasta produce water with ages of 30 years or more. One domestic well (Old Stage Rd) produced pre-modern groundwater.

The high elevation springs on the slopes of Mt Shasta deliver water that is very young (0-5 years), but the contribution of recent snowmelt was at most 25% when sampled in May 2015. The tritium model age of the McCloud Intake spring was 4 years.

The Big Springs complex in the City of Mt Shasta has multiple discharge locations over a relatively small area, comprising large and small discharges totaling approximately 20 cfs. Field parameters such as discharge temperature and EC differ significantly at the different discharge locations, suggesting discrete flow paths with differing water-rock interactions. Interestingly, however, $\delta^{18}O$ values are not significantly different, suggesting similar recharge elevations. Sulfur-35 was detected in the main spring outlet in September, but the fraction of recent precipitation could not be quantified. Sodium-22 results also indicate an age of more than 5 years. The tritium activity in the main spring outlet corresponds to 25 years of decay, or a mixture of modern and pre-modern water. Two other outlets have lower activities, which must be the result of mixing between modern and pre-modern groundwater, or discrete flow paths with differing travel times. The fourth sampled Big Springs outlet produced entirely pre-modern groundwater.

3.4 Spatial Analysis of Land Cover, Precipitation, Evapotranspiration and Groundwater Recharge Elevation

Stable isotope and noble gas results point to a groundwater recharge elevation of 2000 m to 2900 m. To substantiate this finding, spatial data of land use, precipitation and evapotranspiration were analyzed. High resolution (~10 m) land cover data (National Land Cover Dataset obtained from the Multi-Resolution Land Characteristic Consortium, www.mrlc.gov; Homer et al., 2015) was analyzed for the southwestern quadrant of Mt Shasta where all analyzed wells (except Beaughan Spring and Legacy Stone) are located (Figure 20). The proposed groundwater recharge elevation band is highlighted in this figure by black contours at 2000m and 2900m. However, the local topography and meteorology result in strong differences between the windward (south west) and leeward (north east) side of Mt Shasta in terms of land cover, precipitation and temperature. The spatial analysis was limited to a 14 km radius, approximately the distance from the summit to the furthest wells, and also to the drainage system discharging at Big Springs in the city of Mt Shasta.

Below 2250 m elevation, forest (dark green on Figure 20) is the dominant land cover. Between 2250 m and 2500 m elevation, forest is replaced by barren soil (gray on Figure 20) and increasingly above 3000 m by perennial snow (light blue on Figure 20). Despite the large proportion of barren land above 2500 m, the total area of barren land is limited, because the total surface area quickly decreases with increasing elevation. The blue box in Figure 21 outlines the elevation range of recharge to the wells derived from stable isotopes and noble gas results. Within this range, forest occupies 57% of land area, and barren land 35%. Including the entire elevation range above 2000 m (assuming that higher elevation recharge also contributes) the ratios change to 46% and 44% respectively. The lack of recharge from lower forest-covered elevations may result from high evapotranspiration on forested slopes limiting water availability for recharge and point to an important role for barren land with limited evapotranspiration in controlling recharge on Mt Shasta. The loss of barren land on Mt Shasta to forest encroachment in a warming climate may have a significant effect on recharge under future climate change conditions.

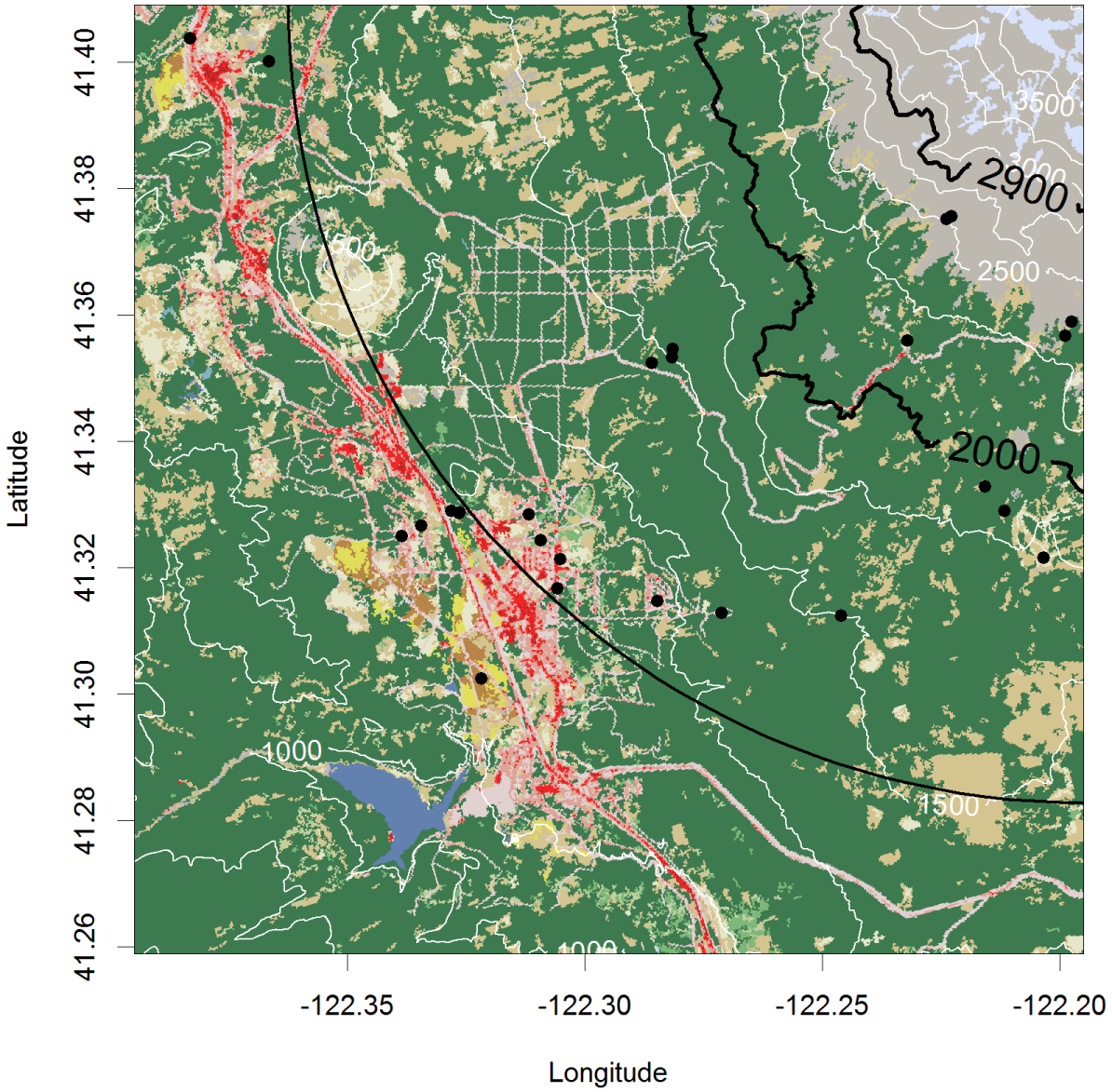

Figure 20: Land cover for selected spatial area, with well and spring locations (black symbols), 250m elevation contours, and the 14 km radius. The proposed groundwater recharge elevation band is highlighted in this figure by black contours at 2000m and 2900m. (Red: developed, green: forest, brown: shrubs, grey: barren soil, light blue: snow)

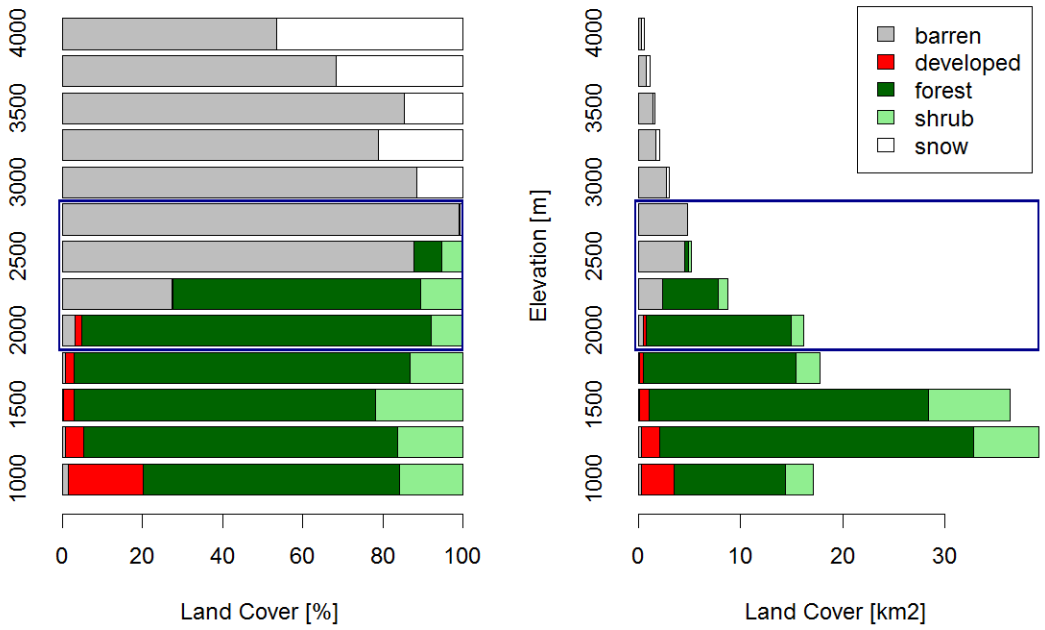

Figure 21: Land cover on south west quadrant of Mt Shasta within a 14 km radius, proportional within elevation ranges (left) and total (right).

The elevation of recharge on Mt Shasta was examined independently by combining PRISM data (PRISM Climate Group, 2016; accessed 2016) for spatially predicted precipitation (800 m resolution) with estimates of evapotranspiration based on normalized difference vegetation index (NDVI) data (10 m resolution data from MODIS NDVI Data for the Conterminous US: 2000-2014; Spruce et al., 2016). Evapotranspiration estimates were based on a regression analysis between annual average NDVI and flux tower measurements of evapotranspiration in the Southern Sierra Critical Zone Observatory in the southern Sierra Nevada (Goulden et al., 2012; Goulden and Bales, 2014)

$$ET\ [mm/yr] = 100.3 * \exp(2.8599 * NDVI)$$

While the scale and location of Mt Shasta and the Southern Sierra Critical Zone Observatory (Goulden et al., 2012; Goulden and Bales, 2014) are different, their climates, ecosystems and elevation ranges are similar. The results of the regression estimates are used here as qualitative indicators of recharge elevation, rather than quantitative estimates of recharge rates.

Elevation within the sector of radius 14 km (southwestern quadrant) of Mt Shasta varies between 1000 m and 4100 m. PRISM predicted precipitation is strongly correlated with elevation, varying from 1100 mm/yr to 2300 mm/yr at the summit. Over that range, mean annual air temperature decreases from 11 °C to -7 °C. Evapotranspiration estimates vary from approximately 700 mm/yr at the base of the mountain to slightly over 100 mm/yr above 2750 m. The strong decrease in ET around 2500 m coincides with the transition from forest to barren land (Figure 23 left). The difference between precipitation and evapotranspiration (P - ET) is available for groundwater recharge and runoff. (Because of very limited surface water flows, P - ET mainly infiltrates rather

than going to runoff.) The combined patterns of P and ET (Figure 22, bottom right) result in a strong contrast of high water availability (blue) above 2500 m and low water availability (red) below 2000 m.

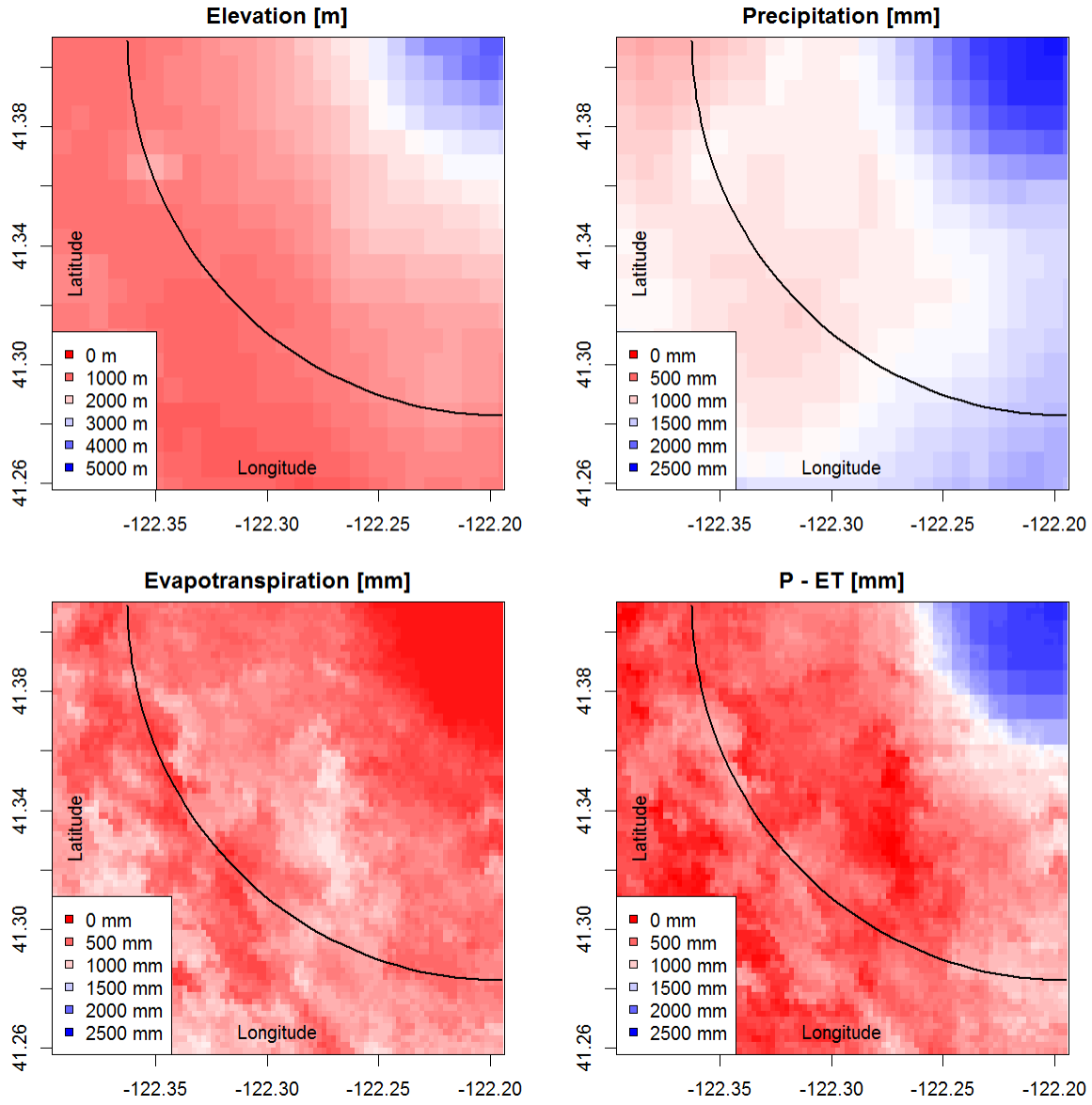

Figure 22: Maps showing elevation, annual precipitation (P), annual evapotranspiration (ET) and annual precipitation excess (P-ET), with a 14-km radius from the summit shown as a back line. Elevation and precipitation rate (top left and right, PRISM data, 800 m resolution) show a strong correlation. Evapotranspiration based on MODIS NDVI (bottom left) is higher at lower elevations but limited in range. Precipitation minus evapotranspiration shows a stark contrast between high elevation barren land and snow cover (above 2500 m) and lower elevation forest cover.

A bar graph of precipitation and ET shows that below 2000m, about 60% of precipitation is lost to evapotranspiration, while less than 10% is lost above 2500m. Net recharge (P-ET) rates increase from 550 mm below 1500 m to 1000 mm at 2000 m and 2000 mm above 3000 m. Because of the large proportion of land area at lower elevations, the average P-ET is 800 mm (Figure 23).

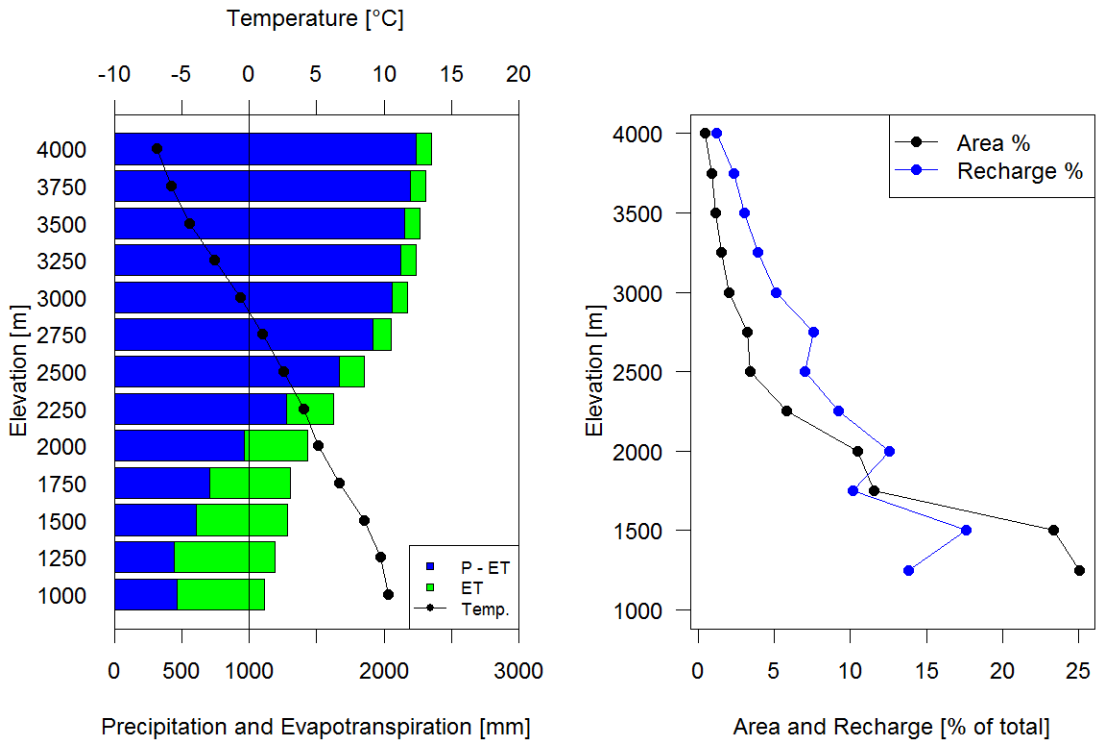

Figure 23: Mean annual precipitation and temperature for 250 m elevation bins within the 14-km radius in the southwest quadrant of Mt. Shasta (left). The blue bar represents recharge (precipitation minus evapotranspiration), the green bar represents evapotranspiration (ET), the sum being the total precipitation (P).Land area (black) and recharge (= P-ET, blue) as a percent of total area and recharge within the 14-km radius in the southwest quadrant of Mt. Shasta (right).

Taking land area into account, it becomes clear that lower elevation bands contribute a larger percentage to total groundwater recharge. Within the 14 km radius, 70% of the land area is below 2000 m and less than 13% of the area is above 2500 m. The distribution of total precipitation is comparable (63% below 2000 m and 19% above 2500 m). Groundwater recharge (estimated as the difference between total precipitation and evapotranspiration) is shifted to higher elevations because of the higher precipitation and lower evapotranspiration rates at higher elevations. Groundwater recharge, however, is still dominated by recharge at lower elevations with more than 50% of recharge is estimated to occur below 2000 m. The average recharge elevation within the 14 km radius, weighted by the fractional recharge contributions, is 2200 m. This estimated elevation is above 2000 m, in agreement with the stable isotopes and noble gas results. Wells and springs that indicate higher recharge elevations are possibly fed by features that recharge a narrow, shallow system at higher elevations and do not mix with lower elevation recharge. It is also possible that this first approximation of recharge contributions on Mt Shasta underestimates evapotranspiration from forest at lower elevations and thereby overestimates recharge contributions at lower recharge elevations. This study's finding that elevations above 2400 m are disproportionally important to groundwater recharge and stream discharge is consistent with observations in the Southern Sierra Critical Zone Observatory (Goulden et al., 2012; Goulden and Bales, 2014).

ACKNOWLEDGEMENTS

We thank the engaged community of Mt Shasta, for their cooperation and support, in particular Meadow Fitton and Raven Stevens. A special thanks to the private well owners, Roseburg, Weed, Mt Shasta and McCloud, who granted us permission to sample their wells, and provided us with invaluable information about the hydrology of Mt Shasta. This study was funded by the California Water Boards Groundwater Ambient Monitoring and Assessment Special Studies program.

REFERENCES

GAMA Project reports are available on the State Water Board GAMA website: http://www.swrcb.ca.gov/water_issues/programs/gama/report_depot.shtml

Alikhani J., Deinhart A., Visser A., Bibby R., Purtschert R., Moran J., Arash Massoudieh and Esser B. K. (2016) Nitrate vulnerability projections from Bayesian inference of multiple groundwater age tracers. *Journal of Hydrology* **in press**, **corrected proof**. Available at: http://www.sciencedirect.com/science/article/pii/S0022169416302098.

Belitz K., Dubrovsky N. M., Burow K., Jurgens B. and Johnson T. (2003) *Framework for a Ground-Water Quality Monitoring and Assessment Program for California*., U.S. Geological Survey Water Resources Investigations Report 03-4166. Available at: http://pubs.usgs.gov/wri/wri034166/.

Belitz K., Jurgens B., Landon M. K., Fram M. S. and Johnson T. (2010) Estimation of aquifer scale proportion using equal area grids: Assessment of regional scale groundwater quality. *Water Resour. Res.* **46**, W11550.

Blackwell D. D., Steele J. L., Frohme M. K., Murphey C. F., Priest G. R. and Black G. L. (1990) Heat flow in the Oregon Cascade Range and its correlation with regional gravity, Curie point depths, and geology. *J. Geophys. Res.* **95**, 19475–19493.

Blodgett J. C., Poeschel K. R. and Thornton J. L. (1988) *A water-resources appraisal of the Mount Shasta area in northern California, 1985*., U.S. Geological Survey Water-Resources Investigations Report 87-4239. Available at: http://pubs.er.usgs.gov/publication/wri874239 [Accessed May 31, 2016].

California DWR (2003) *California's Groundwater*., California Department of Water Resources Bulletin 118 (updated 2003). Available at: http://www.water.ca.gov/groundwater/.

California SWRCB (2016) *Water Conservation Portal - Conservation Reporting*., California State Water Resources Control Board. Available at: http://www.waterboards.ca.gov/water_issues/programs/conservation_portal/conservation_reporting.shtml#monthly_archive [Accessed March 20, 2016].

Clarke W. B., Jenkins W. J. and Top Z. (1976) Determination of tritium by mass spectrometric measurement of 3He. *The International Journal of Applied Radiation and Isotopes* **27**, 515–522.

Deeds D. A., Kulongoski J. T. and Belitz K. (2012) Assessing California Groundwater Susceptibility Using Trace Concentrations of Halogenated Volatile Organic Compounds. *Environmental Science & Technology* **46**, 13128–13135.

Epstein S. and Mayeda T. K. (1953) Variation of O-18 content of waters from natural sources. *Geochim. Cosmochim. Acta* **4**, 213–224.

Fram M. S. and Belitz K. (2011) Occurrence and concentrations of pharmaceutical compounds in groundwater used for public drinking-water supply in California. *Science of the Total Environment* **409**, 3409–3417.

Goulden M. L., Anderson R. G., Bales R. C., Kelly A. E., Meadows M. and Winston G. C. (2012) Evapotranspiration along an elevation gradient in California's Sierra Nevada. *JGR* **117**, G03028.

Goulden M. L. and Bales R. C. (2014) Mountain runoff vulnerability to increased evapotranspiration with vegetation expansion. *PNAS*, 201319316.

Harms, P. A., Visser A., Moran J. E. and Esser B. K. (2016) Distribution of tritium in precipitation and surface water in California. *Journal of Hydrology* **534**, 63-72.

Heaton T. H. E. and Vogel J. C. (1981) Excess air in groundwater. *J. Hydrol.* **50**, 201–216.

Homer C., Dewitz J., Yang L., Jin S., Danielson P., Xian G., Coulston J., Herold N., Wickham J. and Megown K. (2015) Completion of the 2011 National Land Cover Database for the Conterminous United States – Representing a Decade of Land Cover Change Information. *Photogrammetric Engineering & Remote Sensing* **81**, 345–354.

Jurgens B. C., Fram M. S., Belitz K., Burow K. R. and Landon M. K. (2010) Effects of Groundwater Development on Uranium: Central Valley, California, USA. *Ground Water* **48**, 913–928.

Landon M., Green C., Belitz K., Singleton M. and Esser B. (2011) Relations of hydrogeologic factors, groundwater reduction-oxidation conditions, and temporal and spatial distributions of nitrate, Central-Eastside San Joaquin Valley, California, USA. *Hydrogeology Journal* **19**, 1203–1224.

Manga M. and Kirchner J. W. (2004) Interpreting the temperature of water at cold springs and the importance of gravitational potential energy. *Water Resour. Res.* **40**, W05110.

Miller C. D. (1980) *Potential hazards from future eruptions in the vicinity of Mount Shasta Volcano, Northern California*., U.S. Geological Survey Bulletin 1503, Reston, VA. Available at: http://pubs.er.usgs.gov/publication/b1503 [Accessed May 10, 2016].

Moran J., Ruiz R., Ford T., Singleton M., Esser B. K., Soto G. T., Velsko C. and Hillegonds D. (2008) *California GAMA Program: Development of a Field Deployable Dissolved Gas Extraction Apparatus*., Lawrence Livermore National Laboratory, LLNL-TR-407175.

Nathenson M., Thompson J. M. and White L. D. (2003). *Slightly thermal springs and non-thermal springs at Mount Shasta, California: Chemistry and recharge elevations.* Journal of Volcanology and Geothermal Research **121** (1–2): 137-153.

Planert M. and Williams J. S. (1995) *Groundwater Atlas of the United States: California, Nevada by Michael Planert and John S. Williams*., U.S. Geological Survey HA 730-B. Available at: http://pubs.usgs.gov/ha/ha730/ch_b/index.html.

PRISM Climate Group (2016) *PRISM Gridded Climate Data*., Oregon State University. Available at: http://prism.oregonstate.edu.

Rose T. P. and Davisson M. L. (1996). "Radiocarbon in Hydrologic Systems Containing Dissolved Magmatic Carbon Dioxide." Science **273**(5280): 1367-1370.

Singleton M. J. and Moran J. E. (2010) Dissolved noble gas and isotopic tracers reveal vulnerability of groundwater in a small, high-elevation catchment to predicted climate changes. *Water Resources Research* **46**, 1–18 (DOI 10.1029/2009wr008718).

Spruce J. P., Gasser G. E. and Hargrove W. W. (2016) *MODIS NDVI Data, Smoothed and Gap-filled, for the Conterminous US: 2000-2014*., ORNL Distributed Active Archive Center. Available at: http://dx.doi.org/10.3334/ORNLDAAC/1299.

State of California (2014) *Sustainable Groundwater Management Act (SGMA)*., California Legislature SB 1319 (Pavley), SB 1168 (Pavley), and AB 1739 (Dickinson). Available at: http://www.water.ca.gov/cagroundwater/index.cfm.

St-Jean G. (2003) Automated quantitative and isotopic (C-13) analysis of dissolved inorganic carbon and dissolved organic carbon in continuous-flow using a total organic carbon analyser. *Rapid Communications in Mass Spectrometry* **17**, 419–428.

Surano K. A., Hudson G. B., Failor R. A., Sims J. M., Holland R. C., Maclean S. C. and Garrison J. C. (1992) Helium-3 mass spectrometry for low-level tritium analysis of environmental samples. *J. Radioanal. Nucl. Chem.-Artic.* **161**, 443–453.

Uriostegui S. H., Bibby R. K., Esser B. K. and Clark J. F. (2015) Analytical Method for Measuring Cosmogenic 35S in Natural Waters. *Anal. Chem.* **87**, 6064–6070.

USDA (2012) *USDA Plant Hardiness Zone Map*., U.S. Department of Agriculture. Available at: http://planthardiness.ars.usda.gov.

Visser A., Bibby R. K., Moran J. E., Singleton M. J. and Esser B. K. (2015) *California GAMA Special Study: Development of a Capability for the Analysis of Krypton-85 in Groundwater Samples (Draft)*., Lawrence Livermore National Laboratory LLNL-TR- 665865.

Visser A., Moran J. E., Hillegonds D., Singleton M. J., Kulongoski J. T., Belitz K. and Esser B. K. (2016) Geostatistical analysis of tritium, groundwater age and other noble gas derived parameters in California. *Water Research* **91**, 314–330.

Visser A., Singleton M. J., Hillegonds D. J., Velsko C. A., Moran J. E. and Esser B. K. (2013) A membrane inlet mass spectrometry system for noble gases at natural abundances in gas and water samples. *Rapid Communications in Mass Spectrometry* **27**, 2472–2482.

Wagner D. L. and Saucedo G. J. (1987) *Geologic map of the Weed quadrangle (Scale 1:250,000)*., California Division of Mines and Geology: Regional Geologic Map Series Map No. 4A. Available at: http://www.quake.ca.gov/gmaps/RGM/weed/weed.html#.

Welhan J. A., Poreda, R. J., Rison W. and Craig H. (1988). "Helium isotopes in geothermal and volcanic gases of the western United States, I. Regional variability and magmatic origin." Journal of Volcanology and Geothermal Research **34**(3): 185-199.

Table 1: Sample Location and Field Data

Sample	Location	Type	Sample Date	Elevation m	Latitude °	Longitude °	Temperature °C	Conductivity µS/cm	pH	DO mg/L	ORP
111459	Bunny Flat snow	Snow	5/2/2015	2140	41.356	-122.232					
111960	Mt Shasta Snow 1	Snow	2/14/2016	1554	41.341	-122.274					
111961	Mt Shasta Snow 2	Snow	2/14/2016	1835	41.339	-122.259					
111962	Mt Shasta Snow 3	Snow	2/14/2016	2143	41.356	-122.233					
111963	Mt Shasta Snow 4	Snow	2/14/2016	2448	41.371	-122.228					
111964	Mt Shasta Snow 5	Snow	2/14/2016	2758	41.374	-122.208					
111965	Mt Shasta Snow 6	Snow	2/14/2016	3069	41.384	-122.206					
111439	Mt Shasta Big Springs	Spring	4/28/2015	1085	41.3287	-122.3264	7.27	80	6.5	12.28	-55.2
111440	Mt Shasta Big Springs B	Spring	4/28/2015	1085	41.3281	-122.3280	10.56	21.9		11.68	-27.2
111441	Mt Shasta Big Springs C	Spring	4/28/2015	1085	41.3289	-122.3281	9.61	12.2		11.41	-23.2
111442	Mt Shasta Big Springs D	Spring	4/28/2015	1085	41.3290	-122.3275	9.42	11.7		11.01	-1.7
111444	McCloud Intake Spring	Spring	4/29/2015	1396	41.318	-122.117	4.6		7.2	14.13	-16.2
111449	Beaughan Springs	Spring	4/30/2015	1140	41.421	-122.356	9.8	101.7	6.94	9.67	
111453	Mt Shasta Cold Spring	Spring	5/1/2015	1298	41.313	-122.271	7	42.04	6.92	10.09	4.4
111714	McGinnis Spring	Spring	9/17/2015	1878	41.333	-122.216	5.2	56.07	6.95	9.62	9.3
111718	Big Springs Main	Spring	9/18/2015	1123	41.3287	-122.3264	7.2	88		10.3	
111719	Big Springs 2	Spring	9/18/2015	1094	41.3289	-122.3281	10.1	142.5		4.1	
111720	Big Springs 3	Spring	9/18/2015	1094	41.3281	-122.3280	9.4	131.4		8.98	
111722	Panther Spring	Spring	9/18/2015	2346	41.359	-122.198	6	15.39		9.53	
111723	Horse Camp Spring 1	Spring	9/18/2015	2509	41.375	-122.224	5.3	13.51		11.6	
111724	Horse Camp Spring 2	Spring	9/18/2015	2542	41.376	-122.223	5.4	27.49		10.8	
111445	McCloud R at Lower Falls	Surface Water	4/29/2015	1189	41.314	-122.107	11.97	82		11.92	-30.8
111450	Beaughan Creek at Roseburg Bridge	Surface Water	4/30/2015	1134	41.422	-122.357					
111460	Panther Meadow Creek	Surface Water	5/2/2015	2304	41.357	-122.199	2.3	14.12	7.26	10.44	-14.3
111715	Big Canyon Creek Middlefork	Surface Water	9/17/2015	1500	41.312	-122.246	5.6	49.76	6.71	11.38	22.5
111437	Redwood Rd	Domestic	4/28/2015	1146	41.328	-122.312	9.07	87	7.34	2.08	-53.7
111438	Butte Ave	Domestic	4/28/2015	1134	41.324	-122.309	9.69	80		14	
111443	Pine Grove Dr	Domestic	4/28/2015	1085	41.327	-122.334	11.88	25.3		10.22	1.2
111451	Legacy Stone Property	Domestic	4/30/2015	1146	41.422	-122.352	13.7	152.5	6.9	9.41	5.6
111455	Shasta Acres Rd	Domestic	5/1/2015	1225	41.315	-122.285	9.5	87.22	7	9.71	0.2
111456	Highland Drive	Domestic	5/1/2015	1085	41.325	-122.339	12	162.8	6.8	8.28	11.4
111457	Old Stage Rd	Domestic	5/1/2015	1036	41.303	-122.322	11.8	121.6	7.22	9.45	-12.6
111458	McBride Campground Well	Domestic	5/2/2015	1483	41.355	-122.282	7.9	68.8	6.96	9.3	2.2
111712	Ski Park 1	Domestic	9/17/2015	1821	41.322	-122.204	6	86.29	7.18	10.23	-1.8
111713	Ski Park 2	Domestic	9/18/2015	1805	41.329	-122.212	5.6	52.91	6.22	10.26	
111716	Redwood Rd	Domestic	9/17/2015	1146	41.328	-122.312	8.6	10.16	7.01	11	5.1
111717	Shasta Retreat	Domestic	9/17/2015	1461	41.352	-122.286	6.7	65.66	6.57	8.43	30.1
111721	McBride Campground Well	Domestic	9/17/2015	1483	41.355	-122.282	8.1	68.35		9.46	
111446	Gazelle Well	Public Supply	4/29/2015	1134	41.404	-122.383	12.7	109		11.4	11.4
111447	Mazzei Well	Public Supply	4/29/2015	1158	41.400	-122.367	12.43	159		8.85	41
111452	Mt Shasta Well 01	Public Supply	5/1/2015	1122	41.317	-122.306	9	96.21	6.98	7.65	1.3
111454	Mt Shasta High School Well	Public Supply	5/1/2015	1128	41.321	-122.305	8	81.4	7.2		2.5

Table 2: Stable Isotopes of Water ($\delta^{18}O$ and $\delta^{2}H$)

Sample	Location	$\delta^{18}O$ ‰	$\delta^{2}H$ ‰	Sample Elevation m	$\delta^{18}O$ Recharge Elevation m	$\delta^{2}H$ Recharge Elevation m	Elevation Loss m
111459	Bunny Flat snow	-12.7	-95.6	2140	1934	2181	
111960	Mt Shasta Snow 1	-10.5	-66.4	1554	878	445	
111961	Mt Shasta Snow 2	-12.0	-81.7	1835	1621	1349	
111962	Mt Shasta Snow 3	-12.3	-89.3	2143	1759	1805	
111963	Mt Shasta Snow 4	-13.5	-93.5	2448	2311	2053	
111964	Mt Shasta Snow 5	-13.8	-99.1	2758	2443	2385	
111965	Mt Shasta Snow 6	-14.5	-106.4	3069	2812	2819	
111439	Mt Shasta Big Springs	-14.4	-105.7	1085	2767	2778	1682
111440	Mt Shasta Big Springs B	-14.4	-106.1	1085	2761	2804	1676
111441	Mt Shasta Big Springs C	-14.3	-104.5	1085	2713	2709	1628
111442	Mt Shasta Big Springs D	-14.2	-104.9	1085	2669	2732	1584
111444	McCloud Intake Spring	-13.1	-93.3	1396	2119	2041	723
111449	Beaughan Springs	-14.6	-106.6	1140	2834	2832	1694
111453	Mt Shasta Cold Spring	-13.9	-98.5	1298	2514	2349	1216
111714	McGinnis Spring		-92.1	1878		1970	-
111718	Big Springs Main	-14.7	-104.6	1123	2870	2712	1747
111719	Big Springs 2	-14.6	-104.8	1094	2841	2727	1748
111720	Big Springs 3	-14.5	-107.0	1094	2809	2857	1715
111722	Panther Spring	-13.7	-99.7	2346		2423	-
111723	Horse Camp Spring 1	-14.5	-105.5	2509	2777	2764	267
111724	Horse Camp Spring 2	-14.7	-107.1	2542	2914	2863	372
111445	McCloud R at Lower Falls	-11.7	-83.7	1189	1478	1470	289
111450	Beaughan Creek at Roseburg Bridge	-14.4	-105.7	1134	2745	2781	1611
111460	Panther Meadow Creek	-13.0	-93.5	2304	2097	2054	-
111715	Big Canyon Creek Middlefork		-98.3	1500		2340	-
111437	Redwood Rd	-12.9	-94.9	1146	2031	2136	885
111438	Butte Ave	-13.5	-99.0	1134	2306	2381	1172
111443	Pine Grove Dr	-12.8	-95.0	1085	2001	2144	916
111451	Legacy Stone Property	-14.4	-107.1	1146	2750	2859	1604
111455	Shasta Acres Rd	-13.3	-95.0	1225	2235	2139	1010
111456	Highland Drive	-13.7	-99.9	1085	2395	2431	1310
111457	Old Stage Rd	-14.2	-102.5	1036	2665	2589	1629
111458	McBride Campground Well	-13.3	-97.0	1483	2248	2259	765
111712	Ski Park 1		-93.9	1821		2076	
111713	Ski Park 2		-92.3	1805		1983	
111716	Redwood Rd		-94.1	1146		2087	
111717	Shasta Retreat		-99.7	1461		2419	
111721	McBride Campground Well	-14.0	-102.1	1483	2543	2564	1059
111446	Gazelle Well	-13.1	-95.5	1134	2108	2174	974
111447	Mazzei Well	-14.3	-105.2	1158	2689	2747	1531
111452	Mt Shasta Well 01	-13.8	-101.3	1122	2451	2516	1329
111454	Mt Shasta High School Well	-14.2	-102.0	1128	2633	2561	1506

Table 3: Noble Gases

Sample	Location	Helium Isotope Ratio ($\times 10^{-6}$)	Helium-4 ($\times 10^{-9}$ cm^3STP/g)	Neon ($\times 10^{-9}$ cm^3STP/g)	Argon ($\times 10^{-6}$ cm^3STP/g)	Krypton ($\times 10^{-9}$ cm^3STP/g)	Xenon ($\times 10^{-9}$ cm^3STP/g)
111459	Bunny Flat snow						
111960	Mt Shasta Snow 1						
111961	Mt Shasta Snow 2						
111962	Mt Shasta Snow 3						
111963	Mt Shasta Snow 4						
111964	Mt Shasta Snow 5						
111965	Mt Shasta Snow 6						
111439	Mt Shasta Big Springs						
111440	Mt Shasta Big Springs B						
111441	Mt Shasta Big Springs C						
111442	Mt Shasta Big Springs D						
111444	McCloud Intake Spring						
111449	Beaughan Springs	1.5	49.3	197	361	85.9	12.6
111453	Mt Shasta Cold Spring	1.3	41.5	189	374	88.9	13.4
111714	McGinnis Spring						
111718	Big Springs Main		50.0	227	384	90.8	13.8
111719	Big Springs 2		58.3	229	380	89.0	13.5
111720	Big Springs 3		63.9	235	387	89.9	13.9
111722	Panther Spring		42.1	210	360	86.2	13.2
111723	Horse Camp Spring 1		42.2	206	347	82.1	12.2
111724	Horse Camp Spring 2		40.1	195	335	80.7	11.7
111445	McCloud R at Lower Falls						
111450	Beaughan Creek at Roseburg Bridge						
111460	Panther Meadow Creek						
111715	Big Canyon Creek Middlefork						
111437	Redwood Rd	0.6	178.8	265	396	91.7	12.9
111438	Butte Ave	2.0	50.7	218	379	87.5	12.9
111443	Pine Grove Dr	0.4	624.7	199	360	84.7	12.1
111451	Legacy Stone Property	1.5	40.5	183	356	87.4	12.5
111455	Shasta Acres Rd	2.6	52.3	199	372	91.2	13.6
111456	Highland Drive	0.6	1293.2	192	339	82.5	11.9
111457	Old Stage Rd	7.7	203.7	222	404	95.2	13.6
111458	McBride Campground Well						
111712	Ski Park 1	1.4	40.2	184	359	88.3	13.0
111713	Ski Park 2	1.4	61.1	316	525	112.6	15.1
111716	Redwood Rd						
111717	Shasta Retreat						
111721	McBride Campground Well						
111446	Gazelle Well	1.6	46.1	201	365	85.7	12.5
111447	Mazzei Well	7.0	266.2	206	368	87.4	12.7
111452	Mt Shasta Well 01	5.9	128.0	222	381	89.9	13.3
111454	Mt Shasta High School Well	2.7	54.0	202	374	90.9	13.3

Table 4: Noble Gas Derived Parameters

Sample	Location	Probability	Recharge Elevation	Recharge Temperature		ΔNe	Terrigenic Helium	+/-	R_{ter}	$^3H/^3He$ Age	
		%	m	°C	+/-	%	($\times 10^{-9}$ cm^3STP/g)		Ra	years	+/-
111439	Mt Shasta Big Springs										
111440	Mt Shasta Big Springs B										
111441	Mt Shasta Big Springs C										
111442	Mt Shasta Big Springs D										
111444	McCloud Intake Spring										
111449	Beaughan Springs	73%	2149	5.2	0.8	18%	3.3	1.6	2.2	Terr. He	
111453	Mt Shasta Cold Spring	33%	2700	1.9	0.8	17%	0.0	1.5			
111714	McGinnis Spring										
111718	Big Springs Main	96%	2885	0.7	0.6	41%	0.0	4.1			
111719	Big Springs 2	96%	2677	2.0	0.6	41%	3.7	4.4			
111720	Big Springs 3	83%	2933	0.5	0.6	46%	7.8	4.7			
111722	Panther Spring	75%	2519	2.9	0.5	28%	0.0	3.7			
111723	Horse Camp Spring 1										
111724	Horse Camp Spring 2										
111445	McCloud R at Lower Falls										
111450	Beaughan Creek at Roseburg Bridge										
111460	Panther Meadow Creek										
111715	Big Canyon Creek Middlefork										
111437	Redwood Rd	63%	2175	5.0	0.8	59%	113.4	3.9	0.2	Rad. He	
111438	Butte Ave	49%	2307	4.2	0.8	32%	0.0	1.7		34.6	1.5
111443	Pine Grove Dr	58%	1809	7.2	0.8	17%	578.0	12.6	0.3	Rad. He	
111451	Legacy Stone Property	39%	2160	5.1	0.8	9%	0.0	1.4		10.7	3.3
111455	Shasta Acres Rd	67%	2813	1.2	0.9	23%	6.3	1.6	8.5	Terr. He	
111456	Highland Drive	74%	1664	8.1	0.8	12%	1248.4	25.9	0.4	Rad. He	
111457	Old Stage Rd	2%	2782	1.4	0.9	38%	151.1	4.3	7.2	3H < 1 pCi/L	
111458	McBride Campground Well										
111712	Ski Park 1	56%	2448	3.4	0.8	12%	0.0	1.4		0.0	1.8
111713	Ski Park 2	0%	bad fit	bad fit	-	85%	0.0	2.3		0.0	2.6
111716	Redwood Rd										
111717	Shasta Retreat										
111721	McBride Campground Well										
111446	Gazelle Well	58%	2104	5.4	0.8	20%	0.0	1.5		21.5	1.8
111447	Mazzei Well	67%	2241	4.6	0.8	24%	217.9	5.5	5.9	3H < 1 pCi/L	
111452	Mt Shasta Well 01	73%	2580	2.6	0.8	36%	75.3	2.9	6.5	Terr. He	
111454	Mt Shasta High School Well	40%	2592	2.5	0.8	24%	7.1	1.7	8.3	Terr. He	

Table 5: Cations and Anions

Sample	Location	F	Cl	Br	NO3	PO4	SO4	Na	K	Ca	Mg	Li
		mg/L	mg/L	mg/L	mg/L	mg/L	mg/L	mg/L	mg/L	mg/L	mg/L	mg/L
111459	Bunny Flat snow	0.01	0.49	ND	0.49	ND	0.56	0.59	0.23	0.03	ND	ND
111960	Mt Shasta Snow 1											
111961	Mt Shasta Snow 2											
111962	Mt Shasta Snow 3											
111963	Mt Shasta Snow 4											
111964	Mt Shasta Snow 5											
111965	Mt Shasta Snow 6											
111439	Mt Shasta Big Springs	0.10	1.46	ND	0.81	1.56	0.99	8.18	1.58	13.58	1.07	0.01
111440	Mt Shasta Big Springs B	0.11	18.43	0.55	0.73	1.62	1.14	26.15	1.80	35.46	1.37	0.03
111441	Mt Shasta Big Springs C	0.10	4.81	ND	0.82	1.61	1.00	13.68	1.54	22.74	1.47	0.02
111442	Mt Shasta Big Springs D	0.09	3.99	ND	0.82	1.61	1.06	12.89	1.52	21.45	1.44	0.01
111444	McCloud Intake Spring	0.02	0.44	ND	0.68	1.42	0.72	3.04	1.53	5.38	0.89	0.01
111449	Beaughan Springs	0.22	0.82	ND	1.20	1.64	1.60	10.14	1.29	21.11	1.10	0.02
111453	Mt Shasta Cold Spring	ND	0.39	ND	0.64	ND	0.83	2.74	1.38	4.59	1.02	0.00
111714	McGinnis Spring	0.04	0.35	ND	ND	ND	0.17					
111718	Big Springs Main	0.16	1.21	ND	0.36	0.58	0.65					
111719	Big Springs 2	0.14	3.83	ND	0.57	0.68	0.68					
111720	Big Springs 3	0.13	7.02	ND	0.32	0.54	0.74					
111722	Panther Spring	0.03	0.25	ND	0.29	ND	0.21					
111723	Horse Camp Spring 1	0.03	0.16	ND	0.30	ND	0.20					
111724	Horse Camp Spring 2	0.03	0.13	ND	0.40	ND	0.17					
111445	McCloud R at Lower Falls											
111450	Beaughan Creek at Roseburg Bridge											
111460	Panther Meadow Creek	ND	0.33	ND	0.50	ND	0.57	1.14	0.60	0.53	0.14	ND
111715	Big Canyon Creek Middlefork	0.04	0.35	ND	ND	ND	0.42					
111437	Redwood Rd	0.02	0.75	ND	1.62	1.42	0.61	7.26	2.55	11.49	1.56	0.00
111438	Butte Ave	0.04	0.69	ND	1.43	1.43	0.82	6.99	2.43	9.24	1.29	0.01
111443	Pine Grove Dr	0.02	50.33	0.52	5.81	1.40	3.31	12.80	3.77	39.34	4.38	0.01
111451	Legacy Stone Property	0.24	1.56	1.56	0.88	1.62	3.65	12.53	1.65	37.70	1.67	0.03
111455	Shasta Acres Rd	ND	0.67	ND	1.40	ND	0.79	5.07	2.12	13.11	1.44	0.00
111456	Highland Drive	0.04	13.98	0.52	2.97	1.50	2.22	13.96	2.85	23.66	2.11	0.01
111457	Old Stage Rd	0.01	1.53	ND	0.63	1.47	1.17	9.27	2.44	22.03	1.89	0.00
111458	McBride Campground Well	0.02	0.62	ND	1.02	ND	0.67	4.60	2.28	5.43	1.44	0.00
111712	Ski Park 1	0.05	2.55	ND	14.10	ND	1.95					
111713	Ski Park 2	0.04	0.39	ND	0.01	ND	0.22					
111716	Redwood Rd	0.08	0.60	ND	1.45	0.42	0.25					
111717	Shasta Retreat	0.07	0.85	ND	0.21	ND	0.31					
111721	McBride Campground Well	0.05	0.64	ND	ND	ND	0.24					
111446	Gazelle Well	0.04	6.52	ND	4.98	1.49	1.29	10.09	1.59	13.05	1.78	0.01
111447	Mazzei Well	0.27	8.81	0.53	0.73	1.67	1.68	18.51	1.21	31.88	1.45	0.02
111452	Mt Shasta Well 01	0.04	0.93	ND	0.94	1.43	0.87	6.90	1.77	17.32	1.19	0.01
111454	Mt Shasta High School Well	0.04	0.57	ND	0.91	1.45	0.85	6.26	1.86	13.68	1.23	0.00

Table 6: Carbon Isotopes

Sample	Location	TIC	1/TIC	TOC	δ13C	±	$D^{14}C$	±	Fraction Modern	PMC
		mg/L	L/mg	mg/L	‰	‰	‰	‰	-	%
111459	Bunny Flat snow									
111960	Mt Shasta Snow 1									
111961	Mt Shasta Snow 2									
111962	Mt Shasta Snow 3									
111963	Mt Shasta Snow 4									
111964	Mt Shasta Snow 5									
111965	Mt Shasta Snow 6									
111439	Mt Shasta Big Springs	13.9	0.1	0.3	-10.9	0.04				
111440	Mt Shasta Big Springs B									
111441	Mt Shasta Big Springs C									
111442	Mt Shasta Big Springs D									
111444	McCloud Intake Spring	9.7	0.1	0.2	-15.6	0.02				
111449	Beaughan Springs	19.8	0.1	0.4	-9.8	0.10				
111453	Mt Shasta Cold Spring	10.5	0.1	0.2	-16.0	0.07				
111714	McGinnis Spring	6.9	0.1	0.2	-15.7	0.09				
111718	Big Springs Main	8.6	0.1	0.0	-11.0	0.04				
111719	Big Springs 2	13.5	0.1	0.2	-11.0	0.09				
111720	Big Springs 3	14.7	0.1	0.3	-11.8	0.00	-466.57	2.10	0.53	53
111722	Panther Spring	0.9	1.1	0.0	-14.4	0.23	-10.67	2.83	0.99	99
111723	Horse Camp Spring 1	0.8	1.3	0.0	-6.7	0.01	-12.05	2.59	0.99	99
111724	Horse Camp Spring 2	0.8	1.3	-0.1	-4.7	0.02				
111445	McCloud R at Lower Falls									
111450	Beaughan Creek at Roseburg Bridge									
111460	Panther Meadow Creek	2.7	0.4	0.3						
111715	Big Canyon Creek Middlefork	3.6	0.3	0.1	-13.1	0.11				
111437	Redwood Rd	17.1	0.1	0.5	-14.5	0.03				
111438	Butte Ave	15.3	0.1	0.3	-13.4	0.01				
111443	Pine Grove Dr	17.1	0.1	0.5	-13.8	0.02	-85.39	2.62	0.91	91
111451	Legacy Stone Property	27.4	0.0	0.7	-7.9	0.02	-528.48	1.73	0.47	47
111455	Shasta Acres Rd	13.5	0.1	0.3	-15.1	0.00				
111456	Highland Drive	22.1	0.0	0.5	-14.0	0.03	-93.30	3.11	0.91	91
111457	Old Stage Rd	19.0	0.1	0.5	-12.2	0.05	-431.46	1.97	0.57	57
111458	McBride Campground Well	14.1	0.1	0.3	-15.2	0.01	58.81	3.06	1.06	106
111712	Ski Park 1	4.6	0.2	0.1	-14.4	0.10	73.94	3.07	1.07	107
111713	Ski Park 2	5.0	0.2	0.1	-14.5	0.06				
111716	Redwood Rd	10.4	0.1	0.1	-11.1	0.06				
111717	Shasta Retreat	7.4	0.1	0.2	-14.5	0.03				
111721	McBride Campground Well	7.4	0.1	0.2	-14.9	0.04				
111446	Gazelle Well	16.6	0.1	0.4	-15.4	0.04				
111447	Mazzei Well	21.4	0.0	0.5	-12.6	0.02	-499.67	1.75	0.50	50
111452	Mt Shasta Well 01	15.7	0.1	0.3	-13.0	0.06	-146.92	2.59	0.85	85
111454	Mt Shasta High School Well	13.2	0.1	0.3	-13.6	0.16	-124.23	2.54	0.88	88

Table 7: Sulfur-35

Sample	Location	Sample Date	Activity	95% CI	MDA	Recent Snow	^{35}S Model Age
			mBq/L	mBq/L	mBq/L	%	years
111459	Bunny Flat snow	5/2/2015	3.1	0.9	1.0	100%	0.0
111459A	Bunny Flat snow A		2.8	0.9	0.9	89%	0.0
111459B	Bunny Flat snow B		3.4	0.9	1.0	111%	0.0
111439	Mt Shasta Big Springs	4/28/2015	ND		0.8	< 24%	> 0.5
111440	Mt Shasta Big Springs B						
111441	Mt Shasta Big Springs C	4/28/2015	ND		0.8	< 24%	> 0.5
111442	Mt Shasta Big Springs D						
111444	McCloud Intake Spring	4/29/2015	ND		0.9	< 28%	> 0.4
111449	Beaughan Springs	4/30/2015	ND		0.9	< 29%	> 0.4
111453	Mt Shasta Cold Spring	5/1/2015	ND		0.7	< 22%	> 0.5
111714	McGinnis Spring	9/17/2015	ND		0.6	< 61%	
111718	Big Springs Main	9/18/2015	0.7	0.4	0.5		
111719	Big Springs 2						
111720	Big Springs 3						
111722	Panther Spring	9/18/2015	ND		0.7		
111723	Horse Camp Spring 1	9/18/2015	ND		0.7		
111724	Horse Camp Spring 2						
111445	McCloud R at Lower Falls						
111450	Beaughan Creek at Roseburg Bridge						
111460	Panther Meadow Creek	5/2/2015	2.2	0.7	0.8	70%	0.1
111715	Big Canyon Creek Middlefork	9/17/2015	ND		0.4		
111437	Redwood Rd	4/28/2015	ND		0.7	< 23%	> 0.5
111438	Butte Ave	4/28/2015	ND		0.6	< 19%	> 0.6
111443	Pine Grove Dr	4/28/2015	ND		0.6	< 20%	> 0.5
111451	Legacy Stone Property	4/30/2015	ND		0.7	< 21%	> 0.5
111455	Shasta Acres Rd	5/1/2015	ND		0.8	< 27%	> 0.5
111456	Highland Drive						
111457	Old Stage Rd						
111458	McBride Campground Well	5/2/2015	ND		1.0	< 33%	> 0.4
111712	Ski Park 1	9/17/2015	ND		0.4	< 39%	
111713	Ski Park 2	9/18/2015	ND		0.4	< 42%	
111716	Redwood Rd	9/17/2015	ND		0.4	< 39%	
111717	Shasta Retreat	9/17/2015	ND		0.4	< 41%	
111721	McBride Campground Well	9/17/2015	ND		0.5	< 44%	
111446	Gazelle Well						
111447	Mazzei Well						
111452	Mt Shasta Well 01	5/1/2015	ND		0.8	< 25%	> 0.5
111454	Mt Shasta High School Well	5/1/2015	ND		0.6	< 18%	> 0.6

Table 8: Sodium-22

Sample	Location	Volume m3	Activity mBq	Uncertainty mBq	Sample Activity mBq/m3	Uncertainty mBq/m3	MDA mBq/m3	Recent Snow %	^{22}Na Model Age years
111459	Bunny Flat snow								
111372	Sierra Snow (2014-2015)	0.28	39	10	141	35	39	100%	0.0
112274	Sierra Snow (2015-2016)	0.30	46	9	153	29	32	109%	0.0
111962									
111963									
111964									
111965									
111439	Mt Shasta Big Springs	0.29	ND		ND		34	< 24%	> 5.4
111440	Mt Shasta Big Springs B								
111441	Mt Shasta Big Springs C								
111442	Mt Shasta Big Springs D								
111444	McCloud Intake Spring								
111449	Beaughan Springs	0.37	ND		ND		29	< 21%	> 5.9
111453	Mt Shasta Cold Spring		ND		ND		20	< 14%	> 7.4
111714	McGinnis Spring								
111718	Big Springs Main								
111719	Big Springs 2								
111720	Big Springs 3								
111722	Panther Spring								
111723	Horse Camp Spring 1								
111724	Horse Camp Spring 2								
111445	McCloud R at Lower Falls								
111450	Beaughan Creek at Roseburg Bridge								
111460	Panther Meadow Creek								
111715	Big Canyon Creek Middlefork								
111437	Redwood Rd								
111438	Butte Ave								
111443	Pine Grove Dr								
111451	Legacy Stone Property								
111455	Shasta Acres Rd	1.01	ND		ND		10	< 7%	> 9.8
111456	Highland Drive								
111457	Old Stage Rd								
111458	McBride Campground Well								
111712	Ski Park 1								
111713	Ski Park 2								
111716	Redwood Rd								
111717	Shasta Retreat								
111721	McBride Campground Well								
111446	Gazelle Well								
111447	Mazzei Well								
111452	Mt Shasta Well 01	0.53	ND		ND		19	< 14%	> 7.4
111454	Mt Shasta High School Well	1.01							

Table 9: Tritium

Sample	Location	Activity pCi/L	± pCi/L	MDA pCi/L	Recent Snow %	^{3}H Model age years
111459	Bunny Flat snow	9.0	0.5	0.8	100%	0
111960	Mt Shasta Snow 1					
111961	Mt Shasta Snow 2					
111962	Mt Shasta Snow 3					
111963	Mt Shasta Snow 4					
111964	Mt Shasta Snow 5					
111965	Mt Shasta Snow 6					
111439	Mt Shasta Big Springs	3.0	0.3	0.5	34%	> 12
111440	Mt Shasta Big Springs B	1.1	0.2	0.4	12%	> 12
111441	Mt Shasta Big Springs C	1.2	0.2	0.4	14%	> 12
111442	Mt Shasta Big Springs D	ND		1.2	< 14%	> 60
111444	McCloud Intake Spring	7.3	0.4	0.6	81%	4
111449	Beaughan Springs	3.3	0.3	0.4	36%	> 12
111453	Mt Shasta Cold Spring	6.8	0.5	0.8	76%	5
111714	McGinnis Spring	8.6	0.6	1.0	95%	1
111718	Big Springs Main	3.3	0.2	0.3	37%	> 12
111719	Big Springs 2	1.3	0.1	0.2	15%	> 12
111720	Big Springs 3	1.3	0.1	0.2	14%	> 12
111722	Panther Spring	9.7	0.4	0.7	108%	0
111723	Horse Camp Spring 1	8.8	0.4	0.6	98%	0
111724	Horse Camp Spring 2	9.0	0.4	0.7	100%	0
111445	McCloud R at Lower Falls	5.8	0.4	0.6	65%	8
111450	Beaughan Creek at Roseburg Bridge	3.5	0.3	0.4	39%	> 12
111460	Panther Meadow Creek	8.6	0.4	0.7	96%	1
111715	Big Canyon Creek Middlefork	7.3	0.9	1.5	81%	4
111437	Redwood Rd	4.9	0.5	0.9	55%	11
111438	Butte Ave	6.5	0.5	0.8	72%	6
111443	Pine Grove Dr	5.8	0.3	0.6	65%	8
111451	Legacy Stone Property	3.8	0.3	0.4	42%	> 12
111455	Shasta Acres Rd	6.7	0.5	0.9	74%	5
111456	Highland Drive	4.6	0.3	0.5	51%	12
111457	Old Stage Rd	ND		0.3	< 3%	> 60
111458	McBride Campground Well	6.0	0.2	0.2	67%	7
111712	Ski Park 1	7.6	0.6	1.0	84%	3
111713	Ski Park 2	8.0	0.6	1.0	88%	2
111716	Redwood Rd	5.6	0.6	0.9	63%	8
111717	Shasta Retreat	6.6	0.5	0.9	73%	6
111721	McBride Campground Well	6.3	1.0	1.6	70%	6
111446	Gazelle Well	6.5	0.4	0.7	72%	6
111447	Mazzei Well	0.7	0.2	0.3	8%	> 60
111452	Mt Shasta Well 01	3.9	0.3	0.4	43%	> 12
111454	Mt Shasta High School Well	3.2	0.2	0.4	36%	> 12

Table 10: Krypton-85

Sample	Location	85Kr dpm/cm^{3}Kr	+/-	85Kr % present	+/-	85Kr History year	+/-	^{85}Kr Model Age years	+/-
111459	Bunny Flat snow								
111960	Mt Shasta Snow 1								
111961	Mt Shasta Snow 2								
111962	Mt Shasta Snow 3								
111963	Mt Shasta Snow 4								
111964	Mt Shasta Snow 5								
111965	Mt Shasta Snow 6								
111439	Mt Shasta Big Springs								
111440	Mt Shasta Big Springs B								
111441	Mt Shasta Big Springs C								
111442	Mt Shasta Big Springs D								
111444	McCloud Intake Spring								
111449	Beaughan Springs								
111453	Mt Shasta Cold Spring								
111714	McGinnis Spring								
111718	Big Springs Main								
111719	Big Springs 2								
111720	Big Springs 3								
111722	Panther Spring								
111723	Horse Camp Spring 1								
111724	Horse Camp Spring 2								
111445	McCloud R at Lower Falls								
111450	Beaughan Creek at Roseburg Bridge								
111460	Panther Meadow Creek								
111715	Big Canyon Creek Middlefork								
111437	Redwood Rd	1.0	<	1%	<	< 1966		> 49	
111438	Butte Ave								
111443	Pine Grove Dr								
111451	Legacy Stone Property	67.0	3.0	87%	4%	2011	0.5	4	0.5
111455	Shasta Acres Rd	8.4	1.5	11%	2%	1984	1.5	31	1.5
111456	Highland Drive								
111457	Old Stage Rd								
111458	McBride Campground Well								
111712	Ski Park 1								
111713	Ski Park 2								
111716	Redwood Rd								
111717	Shasta Retreat								
111721	McBride Campground Well								
111446	Gazelle Well								
111447	Mazzei Well								
111452	Mt Shasta Well 01	18.4	10.0	24%	13%	1994	7	21	7
111454	Mt Shasta High School Well	18.2	2.4	24%	3%	1994	0.5	21	0.5

Table 11: Aggregate Groundwater Ages

Sample	Location	^{35}S Model Age	^{22}Na Model Age	^{3}H Model age	^{3}H/^{3}He Age		^{85}Kr Model Age		Aggregate Age
		years	years	years	years	+/-	years	+/-	years
111459	Bunny Flat snow								
111960	Mt Shasta Snow 1								
111961	Mt Shasta Snow 2								
111962	Mt Shasta Snow 3								
111963	Mt Shasta Snow 4								
111964	Mt Shasta Snow 5								
111965	Mt Shasta Snow 6								
111439	Mt Shasta Big Springs	> 0.5	> 5.4	> 12					> 12
111440	Mt Shasta Big Springs B			> 12					> 12
111441	Mt Shasta Big Springs C	> 0.5		> 12					> 12
111442	Mt Shasta Big Springs D			> 60					> 60
111444	McCloud Intake Spring	> 0.4		4					4
111449	Beaughan Springs	> 0.4	> 5.9	> 12					> 12
111453	Mt Shasta Cold Spring	> 0.5	> 7.4	5					> 7.4
111714	McGinnis Spring			1					1
111718	Big Springs Main			> 12					> 12
111719	Big Springs 2			> 12					> 12
111720	Big Springs 3			> 12					> 12
111722	Panther Spring			0					< 1
111723	Horse Camp Spring 1			0	0.0				< 1
111724	Horse Camp Spring 2			0	0.0				< 1
111445	McCloud R at Lower Falls			8					8
111450	Beaughan Creek at Roseburg Bridge			> 12					> 12
111460	Panther Meadow Creek	0.1		1					< 1
111715	Big Canyon Creek Middlefork			4					4
111437	Redwood Rd	> 0.5		11	Terr. He		> 49		> 49
111438	Butte Ave	> 0.6		6	34.6	1.5			33 - 37
111443	Pine Grove Dr	> 0.5		8	Terr. He				
111451	Legacy Stone Property	> 0.5		> 12	10.7	3.3	4	0.5	7 - 14
111455	Shasta Acres Rd	> 0.5	> 9.8	5	Terr. He		31	1.5	29 - 33
111456	Highland Drive			12	Terr. He				
111457	Old Stage Rd			> 60	^{3}H < 1 pCi/L				> 60
111458	McBride Campground Well	> 0.4		7					6-7
111712	Ski Park 1			3	0.0	1.8			0 - 2
111713	Ski Park 2			2	0.0	2.6			0 - 3
111716	Redwood Rd			8	0.0	0.0			> 49
111717	Shasta Retreat			6					
111721	McBride Campground Well			6					6-7
111446	Gazelle Well			6	21.5	1.8			19 - 24
111447	Mazzei Well			> 60	^{3}H < 1 pCi/L				> 60
111452	Mt Shasta Well 01	> 0.5	> 7.4	> 12	Terr. He		21	7	14 - 28
111454	Mt Shasta High School Well	> 0.6		> 12	Terr. He		21	0.5	20 - 22